

EMEP Note 2/2003
Date: July 4, 2003

METEOROLOGISK INSTITUTT
Norwegian Meteorological Institute

Technical Report

Further development of a modelling system able to link hemispheric-regional and local air pollution



Peter Wind, Leonor Tarrasón



Leiv Håvard Slørdal, Sverre Solberg, Bruce Denby, Sam-Erik Walker

ISSN 0804-2446

Preface and acknowledgements

This report presents the status of development of a flexible modelling system capable of describing air pollution transport at different scales and dealing with hemispheric, regional, urban and local air pollution related problems. This is the second report in a series of three that will document the progress and development of a nested modelling system for atmospheric particles and photo-oxidant pollution. This modelling system is the final aim of a national cooperation project between the Norwegian Meteorological Institute (met.no) and the Norwegian Institute for Air Research (NILU) addressed to improve the modelling tools presently used for national pollution control and planning. The results from this project are expected to be useful to the work under the Convention for Long-Range Transboundary Air Pollution because they provide a systematic evaluation of the methodologies used to describe the influence of long-range transport in local/urban areas.

We thank Ivar Lie and Astrid Holstad for their help and contributions to the construction of the interpolated meteorological fields.

We thank Dr. R. Stern, Dr. J. Fath and the organisers of CityDelta for making available the emission data base for the Berlin area.

This work is financed by the Norwegian Ministry of the Environment, the Norwegian Ministry of Fisheries and the Norwegian Pollution Control Authority.

EXECUTIVE SUMMARY

This is the second progress report in a series of three that documents the development of a Norwegian one-way nested modelling system for photo-oxidants and atmospheric particles. The report documents the latest developments within the regional EMEP Unified Model and the urban scale EPISODE Model to allow for a system that couples the study of regional and local air pollution problems.

The two models are at present capable of simulating air pollution transport on successively smaller sub-domains with increasing model resolution. In this sequence of model simulations the necessary boundary conditions for each sub-domain are produced by the previous (coarser) model run. Both models use one-way nesting procedures that rely on updates of the boundary conditions for the finer resolution run, but where the solution within the finer nest do not influence back on the coarser solution. The two models are now coupled as EPISODE can run with EMEP boundary conditions.

This progress report aims at documenting model advances and results from selected sensitivity runs to test the performance of the nesting system. The technical model development that has been necessary to reach this nesting capacity is documented separately for EMEP and EPISODE. While in EMEP the development has concentrated in the analysis of the input data and numerical treatment of the boundary conditions, in EPISODE, the model code has been reformulated in addition to allow for a new vertical coordinate and a new simplified chemistry scheme has been implemented.

A fundamental choice that must be done before starting a nested simulation is the determination of grid sizes and grid resolutions. This choice is determined by the lifetime of the pollution and the type of application in focus but it is often limited by the availability of meteorological and emission data. In meteorological applications, it is common to choose successive grid resolutions increasing with a factor three for each nested grid. In air pollution models the factor three rule may be too restrictive, and the nesting can be achieved more effectively by choosing a larger stride between the nested grids.

The sensitivity tests presented in this report deals with the response of the self nested modelling system to:

- 1) the rate of update of boundary conditions,
- 2) the grid resolution between nested simulations,
- 3) the grid resolution of emissions and,
- 4) the choice of meteorological input data.

The first point involves an evaluation of the importance of long-range transport in the area considered. The rate of update of the boundary concentrations which is required in a nested run depends on the geographical position of the modelling domain, its size and grid resolution and naturally also on the lifetime of the pollution in focus. The smaller the domain is with respect to the pollutant lifetime and typical transport distances, the more important become the influence of boundary conditions and the more often these should be updated. For instance, the sensitivity tests run at Oslo with EMEP Unified shows that O₃, NO₂ and PM₁₀ concentrations in the Oslo domain are all considerably affected by boundary conditions (and

thereby long-range transport). This result is well known for ozone and NO₂ and it is important to note that this is also the case for PM₁₀.

The second point is also relevant for the type of nested simulations that can be carried out for Oslo conditions in the future. The initial results imply that the embedding grid can have a much coarser resolution than first assumed. Only the innermost grid containing the main sources of interest (urban centre for instance), needs to be described with a very high resolution. It has been shown in this report that the EPISODE model applied on a grid with a resolution of 2.5 km and with 50 km EMEP data on the boundaries, gives very similar results as when using a successive nesting with 50-10-5-2.5 km resolution.

It is however important to note that these are only preliminary results valid only for the specific cases tested here. More testing is needed before general conclusions can be drawn. In particular, the future tests must be performed on longer timescales covering both winter and summer months.

The sensitivity tests concerning the effect of resolution of gridded emissions showed, for both the EMEP and the EPISODE models, that close to strong emission sources the effect of improved emission description is clearly important, especially for short lived components like NO₂. This demonstrates the necessity of using high resolution information for the description of urban areas. However, away from the pollution sources the models did not reveal any strong dependence on the resolution of the emissions, clearly indicating that these areas can be well described by rather coarse grids.

A last fundamental question that needs to be analysed is the dependence of the modelling results to the choice of meteorological data. In most of the simulations presented in this work the meteorological data was interpolated down to the different grid resolutions. A more correct approach would be to calculate directly the meteorological data in each grid. This procedure has been applied in the sensitivity tests carried out using the model system Mathew/EPISODE. These tests show that large differences can be expected by changing the description of the meteorology. At met.no different meteorological drivers are presently being evaluated. The testing of HIRLAM50, HIRLAM20, MM5 and ECMWF meteorological data will be a central part in the next phase of this project.

SAMMENDRAG

Dette er den andre rapporten i en serie på tre. Rapporten dokumenterer utviklingen av et enveis nestet modellsystem for beregning av konsentrasjonen av fotooksidanter og luft partikler. Rapporten beskriver videreutviklingen av den regionale EMEP Unified modellen og av byskalamodellen EPISODE. Målet har vært å muliggjøre en kombinert analyse av luftforurensningsproblemer både i regional og lokal skala.

De to modellene kan nå benyttes til å simulere spredning av luftforurensning på gradvis mindre områder (sub-domener), med økende grad av geografisk romlig oppløsning. For hvert nytt modellområde hentes de nødvendige randverdiene fra den foregående beregningen på det utenforliggende (grovere) modellområdet. Begge modellene benytter seg av en såkalt "enveis nesting" teknikk. Dette betyr at løsningene i områdene med finere oppløsning påvirkes av de grovere områdene gjennom randverdiene, men at ingen slik påvirkning skjer den andre veien. Modellene EPISODE og EMEP Unified er nå koblet, og EPISODE kan kjøres med resultater fra EMEP Unified som randverdier.

Denne rapporten har som målsetting å dokumentere modellutviklingen og resultatene fra utvalgte sensitivitetstestinger. Uviklingsarbeidet i både EMEP modellen og EPISODE har vært konsentrert om analyse av inngangsdata og numerisk behandling av randbetingelsene. I tillegg er det gjennomført modellendringer i EPISODE ved at et nytt vertikalt koordinat er lagt inn og at et nytt forenklet kjemi-skjema er blitt implementert. Dokumentasjonen av de tekniske modifikasjonene som er gjennomført for å implementere koblingsfunksjonaliteten, er beskrevet separat for EMEP og EPISODE.

Valg av modellområde og geografisk oppløsning er avgjørende før nestede simuleringer gjennomføres. Det er forurensningens levetid og hva som er hensikten med den aktuelle modellen anvendelsen som avgjør valget, men ofte vil valget begrenses av tilgjengeligheten på meteorologiske - og griddede utslippsdata. I meteorologiske anvendelser er det vanlig å velge suksessivt høyere oppløsning med en faktor på 3 for hvert nestet gitter. I luftforurensningsmodeller kan en faktor på tre være unødig begrensende, og nesting kan gjøres mer effektivt ved å benytte lengre steg mellom de nestede modellgitterne.

Sensitivitetstestene som presenteres i denne rapporten belyser hvordan de nestede modellsystemene reagerer på viktige brukerstyrte parametre som f.eks:

1. hvor ofte randbetingelsene oppdateres,
2. variasjonen i oppløsning mellom ulike koblede områder
3. oppløsningen av utslippsdataene og
4. valg av meteorologiske inngangsdata.

Oppdatering av randbetingelsene henger sammen med betydningen av langtransportbidraget i området som vurderes. Hvor ofte randbetingelsene oppdateres i nestede simuleringer avhenger av geografisk posisjon av modellområdet, dens oppløsning og størrelse og sist men ikke minst av levetiden på forurensning. Når randbetingelsene holdes konstant, ser man at

simuleringen ikke viser de samme toppene i konsentrasjon av NO₂, O₃ og PM₁₀, som når randbetingelsene oppdateres. Jo mindre modellområdet er, desto sterkere blir innflytelsen av randbetingelsene. Dermed øker viktigheten av hyppigere oppdatering av randkonsentrasjonene. Hvilken tidsskala som gir best resultat er dessuten avhengig av avstand til utslippskilden; kortere avstand gjør at oppdatering bør gjøres oftere.

Sensitivitetstestene med EMEP Unified modell viser at konsentrasjonsnivåene av O₃, NO₂ og PM₁₀ i Osloområdet er betydelig påvirket av randbetingelsene; med andre ord av forurensning som skjer utenfor modellområdet. Det vil si at forurensningsnivået har et betydelig langtransportert bidrag. Dette er allment kjent for ozon og NO₂, og det er viktig å understreke at det også gjelder for PM₁₀.

Variasjonen i oppløsning mellom de ulike områder som er koblet er også relevant for framtidige nestede simuleringer for Oslo. De første testresultatene tyder på at de ytterste modellområdene kan ha en langt grovere oppløsning enn først antatt. Bare det innerste modellgitteret, som inneholder de viktigste forurensningskildene (f.eks. byområder), må beskrives med svært høy oppløsning. Det er blitt vist i denne rapporten at EPISODE-modellen, benyttet på et gitter med oppløsning på 2.5 km og med 50 km EMEP data på randen, gir resultater som er svært sammenfallende med de som fremkommer når et fullt nestet system, med 50-10-5-2.5 km oppløsning, benyttes.

Det må likevel understrekes at dette er foreløpige resultater som strengt tatt bare er gyldige for de spesifikke situasjonene som er testet. Flere tester er påkrevd før mer generelle konklusjoner kan trekkes. Det er i denne forbindelse viktig at framtidige tester går over lengre perioder, som dekker både vinter- og sommersituasjoner.

Sensitivitetstestene, som ble gjennomført både med EMEP Unified Model og EPISODE for å belyse effekten av oppløsningen av utlippene, viste at en detaljert utslippsoversikt er av stor betydning i områdene nær utslippskildene. Dette gjelder spesielt for komponenter med kort levetid, som f.eks. NO₂. Testene understreker nødvendigheten av å benytte høy gitteroppløsning når modellen skal anvendes på byområder. Imidlertid viste resultatene også at betydningen av utslippsopløsningen var av langt mindre betydning i områder lenger unna utslippskildene, noe som klart indikerer at disse områdene kan beskrives godt ved hjelp av ganske grove gitteroppløsninger.

Den siste viktige punktet som må testes er effekten av ulike valg av meteorologiske inngangsdata. I de fleste av testene som er presentert i denne rapporten, ble de meteorologiske dataene interpolert ned til de ulike gitteroppløsningene. En mer korrekt fremgangsmåte ville være å beregne de nødvendige dataene direkte i de ulike modell-gitterne. Denne prosedyren er benyttet i sensitivitetstestene som er gjennomført ved bruk av modelsystemet Mathew/EPISODE. Disse testene viser at store forskjeller kan forventes som følge av en endret beskrivelse av de meteorologiske forholdene. Ved met.no blir nå ulike meteorologiske modeller vurdert. Tester med bruk av meteorologiske data fra HIRLAM50, HIRLAM20, MM5 og ECMWF, vil utgjøre en sentral del av den neste fasen i dette prosjektet.

CONTENTS

<i>Preface and acknowledgements</i>	3
EXECUTIVE SUMMARY.....	5
SAMMENDRAG	7
1. Introduction	11
2. Nesting the EMEP Unified Model	13
2.1 Description of the EMEP model one-way nesting system.....	13
2.2 Technical considerations	14
2.2.1 Interpolation of meteorological fields and other input data.....	14
2.2.2 Computational cost	15
2.3 Numerical experiments	16
2.3.1 Oslo in 10 km grid resolution	17
2.3.2 Effect of boundary conditions.....	20
2.3.3 Effect of refined description of emissions	23
3. Model development of the urban scale dispersion model EPISODE	31
3.1 Implementation of the new vertical coordinate transform in EPISODE	31
3.2 Photochemical mechanism in the EPISODE model.....	32
3.2.1. The present chemical routine in EPISODE	33
3.2.2 Evaluation of chemical mechanisms available.....	33
3.2.3 Simplifications of the EMEP mechanism.....	34
3.2.4 Numerical implementation of the new chemical scheme in EPISODE	35
3.3 Development of a self-nested version of EPISODE	38
3.3.1 Summary of the necessary EPISODE changes to allow for self-nesting	38
3.3.2 Idealized test simulations	39
3.3.3 Test experiments with variable topography for the city of Oslo	43
4. The nested EMEP/EPISODE model	45
4.1 The base case experiment	45
4.2 Sensitivity experiments	57
4.3 Conclusions and recommendations based on the Berlin test experiments	60
5. Conclusions and remaining tasks	63

1. Introduction

This report presents the status of development of a flexible modelling system capable of describing air pollution transport at different scales and dealing with hemispheric, regional, urban and local air pollution related problems. This is the second report in a series of three that will document the progress on the development of a one-way nested modelling system for atmospheric particles and photo-oxidant pollution.

This one-way nested modelling system is the final aim of a national cooperation project between the Norwegian Meteorological Institute (met.no) and the Norwegian Institute for Air Research (NILU) addressed to improve the modelling tools presently used for national pollution control and planning.

The results from this project are expected to be useful to different areas of work under the Convention for Long-Range Transboundary Air Pollution. For example, the methods developed here to enable a more flexible choice of model resolution also allow the extension of the model to a hemispheric domain. This is a priority area within the EMEP programme as there is increasing evidence that air pollution, traditionally considered as local or regional such as tropospheric ozone and fine particles, may be transported over very long distances and affect remote environments. It is also expected that the results from this project will facilitate the cooperation with the Working Group of Effects as it would allow more detailed studies of deposition impact over identified problem ecosystem areas.

The models to be applied in this project are the regional scale EMEP Unified Eulerian model (EMEP, Report 1/2003, Berge and Jakobsen, 1998; Olendrzynski et al, 2000) and the urban scale EPISODE model (Grønskei et al., 1993; Walker et al., 1999; Slørdal et al., 2002, 2003). In the first part of this project (Wind et al., 2002), these models have been adapted so as to allow for variable grid resolutions. In this report we document the necessary revisions of the EMEP (section 2) and EPISODE (section 3) models in order to allow for both the self-nesting capability of each of the models and for the coupling of the two models.

In order to demonstrate the level of achievement of the system, several simulations are performed using the new capabilities of the models. The initial results presented here are the first steps towards a more comprehensive study where the influence of different input parameters to local scale simulations are analysed separately. In particular, we are interested in the differences in local scale simulations of particulate matter, nitrogen oxides and ozone when using:

- Different emission data at different scales (aggregated or interpolated)
- Different meteorological drivers (with refined topography or interpolated fields)
- Different boundary conditions and extension of the model domain

This study is expected to result in recommendations about the specifications of a system able to link regional and local air pollution levels.

2. Nesting the EMEP Unified Model

The EMEP models have been traditionally used for the analysis of the transport, chemical transformations and deposition of air pollutants at the regional level (EMEP, 2002). The Unified EMEP Eulerian model has now been developed to allow a flexible choice of the model domain and model resolution, with size of gridcells ranging from 50x50 km² and down to 5x5km². Calculations at different scales are coupled through one-way nesting. This allows the EMEP model to link regional long range transport to urban and local pollution, and in this way determine the influence of background contributions to urban air pollution levels. The description of intercontinental exchange of pollution in a hemispheric scale is also facilitated within the same framework.

The EMEP model has access to meteorological data from several different numerical weather prediction models: HIRLAM50, HIRLAM20, MM5 and ECMWF model. In addition, the Norwegian meteorological institute (met.no) has developed a new interpolation system that ensures the mass conservation properties of the atmospheric flow (Holstad and Lie, 2002). These different meteorological driver data and interpolated fields will be used to study ozone formation and nitrogen oxides levels in Oslo and surrounding areas.

In the first report (Wind et al., 2002) of this project, we presented recent developments of the EMEP model, to allow for a flexible choice of grid resolution. In this second report we document the improvements to the system which make possible the coupling of grids with different resolutions through one-way nesting. The first simulations obtained with the new nesting system are presented in section 2.4.

2.1 Description of the EMEP model one-way nesting system

The main elements in the nesting system of the EMEP Unified Model are now in place. The principles of the system are described in this section.

In a nested run two (or more) grids are defined: a large grid with coarse resolution and a smaller grid with finer resolution. The small grid must be covered by the larger grid, but otherwise there are no limitations in the size or orientation of the small grid.

First the model is run in the large standard (EMEP) grid with Hirlam50 meteorology and EMEP emission data. The calculated concentrations are saved at specific time intervals. The rate of which the concentrations are saved can be defined (dt_nest) as input parameter. All the advected species are stored. In the present version (rv1.6) this represents 56 different chemical species in the UNI-OZONE version, 12 in the UNI-ACID version. The UNI-OZONE version includes in addition 15 short lived species which are not advected and therefore do not need to be stored for the nesting.

Once the relevant data from the large grid is stored, a second run is performed in the small grid. At the start of the run the concentrations on the entire three-dimensional small grid are initialised by the concentrations stored in the first run. After each time interval dt_nest, the concentrations at the lateral boundaries are updated. Between two updates the concentrations at the lateral boundaries are held constant. The update of the concentrations involves a

bilinear horizontal interpolation from the coarse to the fine grid. The system can also interpolate the fields vertically if the two grids have different vertical level definitions.

Since there is no feed-back of the concentrations from the small grid to the larger grid, the system is, at present, a one way-nesting procedure.

2.2 Technical considerations

2.2.1 Interpolation of meteorological fields and other input data

The EMEP Unified Model makes use of several types of input data which must be read by the program at runtime. The most important input files describing the physical processes are: meteorological fields, level of emissions and landuse. In addition comes several other type of data such as emissions factors, lightning, volcanoes, deposition factors etc.

In nested runs several different grids are used and the input data must be made compatible to the actual grid definition.

Interpolating a field involves defining values at new positions where the fields are not defined using surrounding values of the field. Since the interpolated field contain information which is not present in the original field, we have to make assumptions on the properties of the field in order to calculate new values. There is no universal and perfect way of interpolating fields and each method have its advantages and drawbacks, therefore the interpolation method must be selected according to the properties of the field.

For fields like horizontal wind speed there are no special constraints on the values they can be assigned, and the horizontal interpolation can use high order algorithms. For example a bicubic interpolation will ensure a smooth field.

The specific humidity cannot be negative and it cannot be larger than one. A high order interpolation mechanism may result in values which are outside the allowed interval. For fields which are bounded only monotone interpolation algorithms should be used, i.e. methods that will not increase the maximum value of the field or decrease the minimum value. The bilinear and the zeroth order interpolation are monotone.

For the emission fields there is a new constraint: emissions fields cannot be negative, but in addition it is desirable that the total amount of emissions over a given (large) area is conserved. For example the total emissions from a country should not change with the choice of the grid. The interpolation method should then conserve the value of the field integrated over any area. Note that bilinear and zeroth order methods are integral conservative in the case where the new gridcells are a subdivision of the original gridcells (i.e. each gridcell is divided into an integer number of smaller gridcells). In the cases where a grid is rotated or when a gridcell in the fine grid overlaps several gridcells in the coarse grid, more complicated methods (for example numerical integration) have to be used.

Table 1 gives the interpolation method used for the different fields.

Table 1: Interpolation method used for the input fields

Interpolation method	bicubic	Bilinear	Integral conservative
Field	Wind speed Pressure Sigmadot Potential temperature 2 meter temperature Surface flux of sensible heat Surface flux of latent heat	Specific humidity Cloud water content Precipitation Cloud cover Surface stress Topography Landuse	Emissions

The construction of new meteorological fields that can be used as input for model runs presents no major difficulties; however the preparation of meteorological data from a new source represents a large amount of work, because it involves several format or representations and an understanding of the physical content of the data. Not all the fields needed by the air pollution model are standard outputs in meteorological model. For example the three-dimensional description of precipitations is crucial in our model, but only the surface precipitations is usually retained for meteorological purposes.

At met.no a system has been set in place to interpolate the meteorological fields. In this procedure each meteorological field is first transformed in the horizontal direction (flt2flt) where the field is interpolated into the new grid orientation and resolution. Next, the fields are transformed in the vertical direction (eta2eta), in order to adapt the fields to the local topography. The local topography in the fine grid should then be provided to the system.

The system can also include a module which ensures the mass conservation properties of the atmospheric flow (Holstad and Lie, 2002). The effect of this module is to be tested in future runs. In addition to these transformations of the fields, the files containing the data undergo several transformations of formats and representations, to adapt the files to the needs of the different programs and computers.

Meteorological fields for the past years covering the EMEP grid have been stored: 1980, 1985, 1990, 1995, 1996,1997, 1998, 1999, 2000, 2001 are available (Benedictow 2003). Together with the interpolation system, met.no is now able to rapidly produce meteorological fields for any grid within the EMEP area.

2.2.2 Computational cost

A simple nested calculation requires one run in a coarse grid and one run in the nested fine grid. The supplementary CPU usage due to the construction, writing and reading of the concentrations due to the nesting is negligible. The CPU cost depends mostly on the number of gridcells, the length of the run and, indirectly, the grid resolution. The use of a finer grid resolution will require smaller timesteps for the advection routines and will also influence the number of timesteps in the chemical solver. (The timesteps scheme in the chemical solver

routines has recently been modified; see EMEP Report 1/2003.) For the coarse EMEP grid most of the CPU time (about 80%) is spend in the chemical solver. For finer grids the relative time spend in the chemical solver routines decreases, because smaller timesteps must be used for the advection routines, whereas the timesteps for the chemical solver does not need to be decreased as much.

In table 2 we show the key timing parameters for the three grids used in section 2.3. The numbers under “CPU usage” correspond to a parallel run on 36 processors covering one month. The real time for one run is about 1 to 1½ hours (CPU usage divided by the number of processors).

Table 2: Grids and timing parameters for the runs of section 2.3

Grid size	Grid resolution	CPU usage	Master timestep	Number of iterations in chemical solver	Size of the concentration files used for nesting
125x113 EMEP	50x50 km ²	29 hours	1200 s	12	
100x100 Oslo	10x10 km ²	48 hours	360 s	9	1.3 GBytes
100x75 Berlin	5x5 km ²	45 hours	240 s	7	0.4 GBytes

In an off-line nested run the concentrations have to be stored regularly during the run. This represents a large amount of data and storage capacity can be a limitation; for example to store the 56 different concentrations in 20 vertical levels and 125x113 horizontal gridcells every 3 hours during one month necessitates $56 \times 20 \times 125 \times 113 \times (24 \times 30 / 3) = 3.8 \cdot 10^9$ values or 30 Gbytes (in double precision).

Therefore it is preferable to store only the concentrations from gridcells which overlap the small grid. Usually the small grid is only a small fraction of the entire EMEP grid. If storage is still a problem, it would also be possible to store only the concentrations at the lateral boundaries instead of all the values within the three-dimensional subgrid; however this last possibility is not used in our system.

2.3 Numerical experiments

Although the nesting system of the EMEP Unified Model is still under development, some interesting tests can already be performed. The purpose here is not to estimate the performance of the model against measurements, but rather to test the sensitivity of the model to various input parameters. The results of these sensitivity tests will be a good starting point for defining the requirements and specifications of a nesting system.

In all the tests presented in this section, the EMEP-Unified version rv1.6 has been used. The different grids all use the same vertical resolution of 20 vertical levels. In the nested runs, the boundary concentrations are updated every three hours if not otherwise specified.

2.3.1 Oslo in 10 km grid resolution

In this first experiment, the direct influence of the nesting procedure will be tested. In a stable system the results should be affected only by the physical parameters, and the effect of the nesting in itself should be small. In order to test the robustness of the nesting procedure, a grid of dimensions 1000x1000 km² covering the region around Oslo in 10x10 km² resolution is defined. The meteorological and emission fields are obtained by interpolating these data from the coarse EMEP grid (50x50 km²) down to the 10x10 km² resolution grid. The only additional information which is given in the fine grid is the topological information provided to the interpolation routines. Otherwise the physical information in the input data is the same for the calculation in both grids, and differences in concentrations are expected to be due only to numerical effects. The 10x10 km² grid is nested into the larger EMEP grid. Every third hour the concentrations at the boundaries of the small grid are set equal to the concentrations obtained in the large grid.

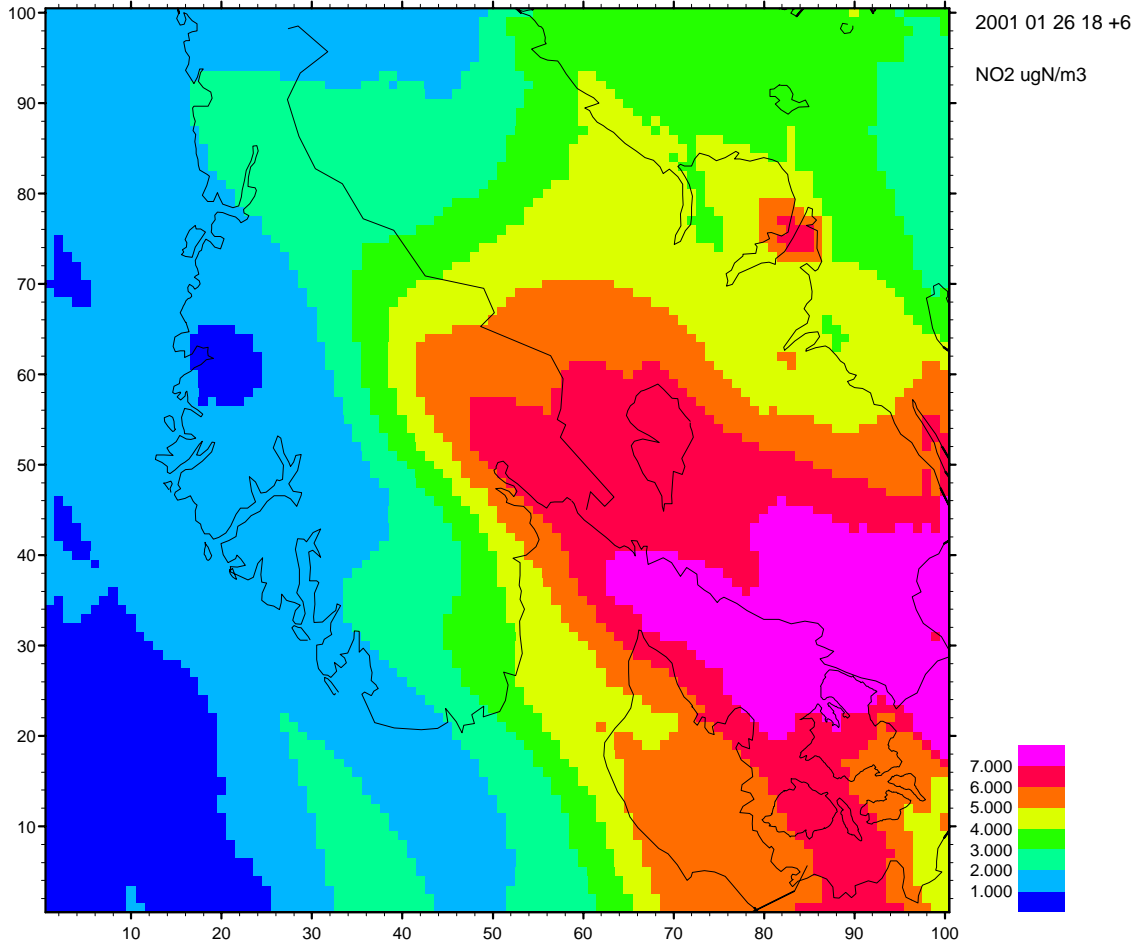


Figure 2.1: Fine 100x100 grid with 10x10 km² resolution covering the region around Oslo. The figure shows the daily NO₂ concentration in µgN/m³ on 26th of January 2001.

In figure 2.1 the area covered by the fine grid with $10 \times 10 \text{ km}^2$ resolution is shown. As an illustration, the concentrations of NO_2 the 26th of January 2001 are represented. In the next figure (2.2) the same area is depicted with the concentrations obtained in the coarse grid with $50 \times 50 \text{ km}^2$ resolution. The concentration distribution in the fine grid is clearly smoother than in the coarse grid, however no new features or higher peaks due to the finer resolution can be observed in this example.

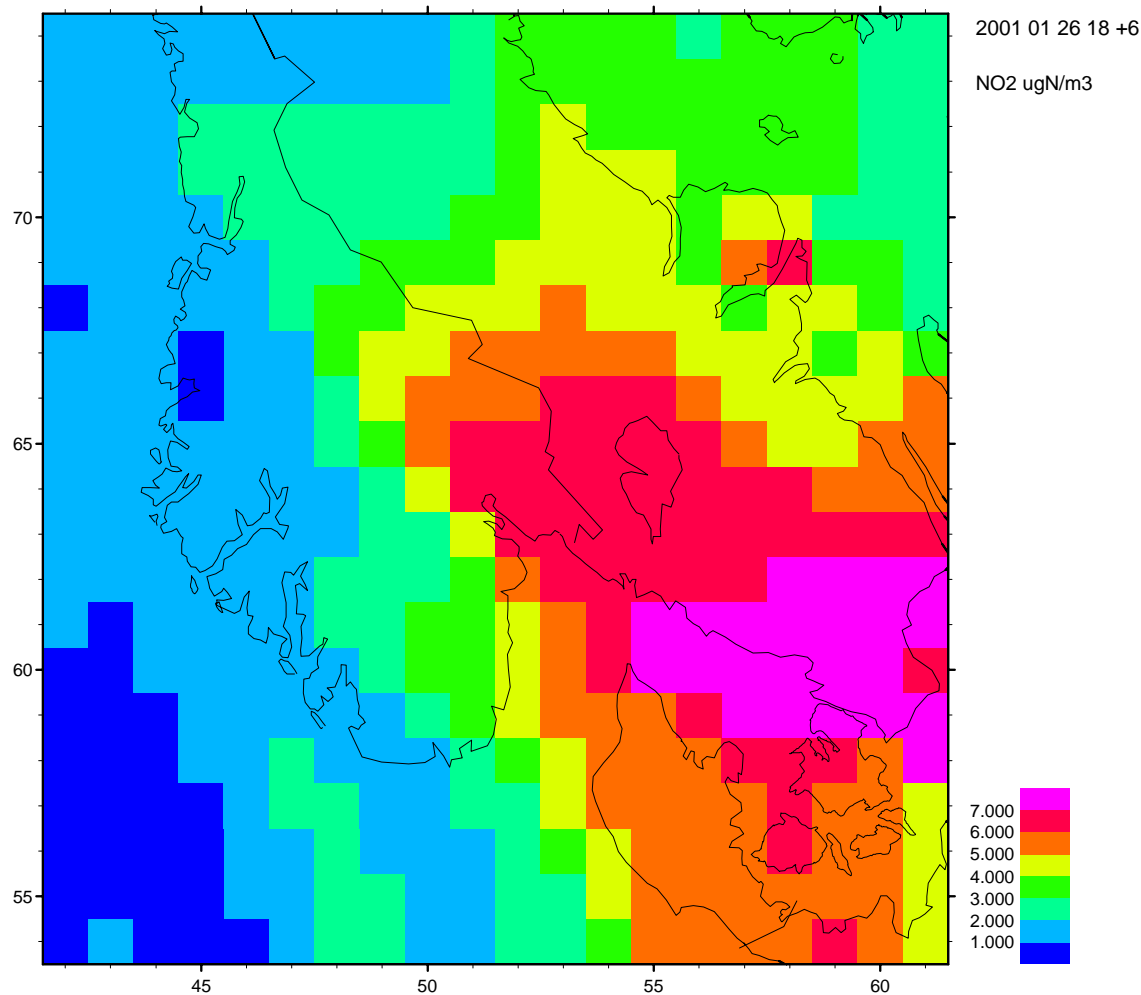


Figure 2.2: Part of the coarse EMEP grid with $50 \times 50 \text{ km}^2$ resolution. The area shown covers the same area as in figure 2.1. The figure shows the daily NO_2 concentrations in $\mu\text{gN}/\text{m}^3$ on 26th of January 2001.

A more detailed comparison can be done by comparing the evolution of the concentrations in Oslo obtained in the two grid resolutions. Figure 2.3, 2.4 and 2.5 show the simulated concentrations of NO_2 , O_3 and PM_{10} respectively in Oslo, January 2001.

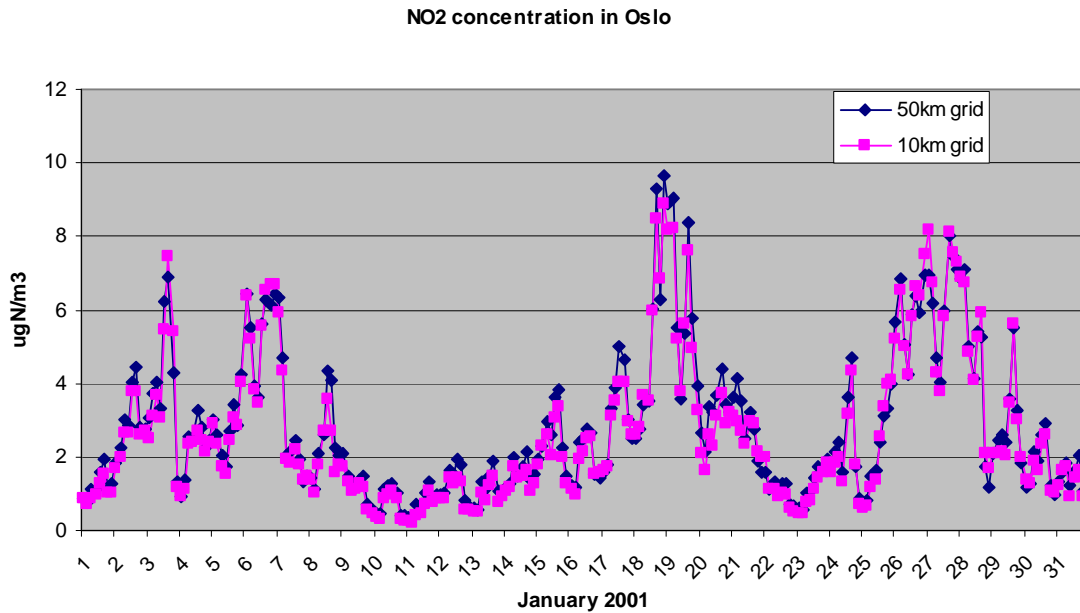


Figure 2.3: Evolution of the NO_2 concentrations ($\mu\text{gN}/\text{m}^3$) in Oslo simulated in two different grids. The values obtained directly in the 50 km grid are compared with the results obtained in a nested grid with 10 km resolution.

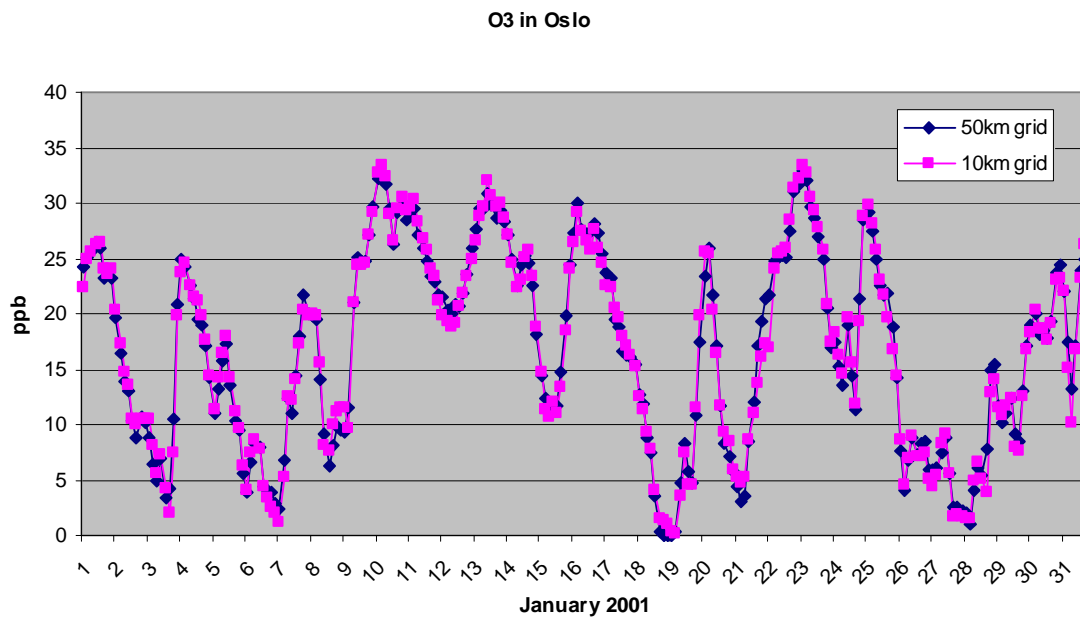


Figure 2.4: Evolution of the O_3 concentrations (ppb) in Oslo simulated in two different grids. The values obtained directly in the 50 km grid are compared with the results obtained in a nested grid with 10 km resolution.

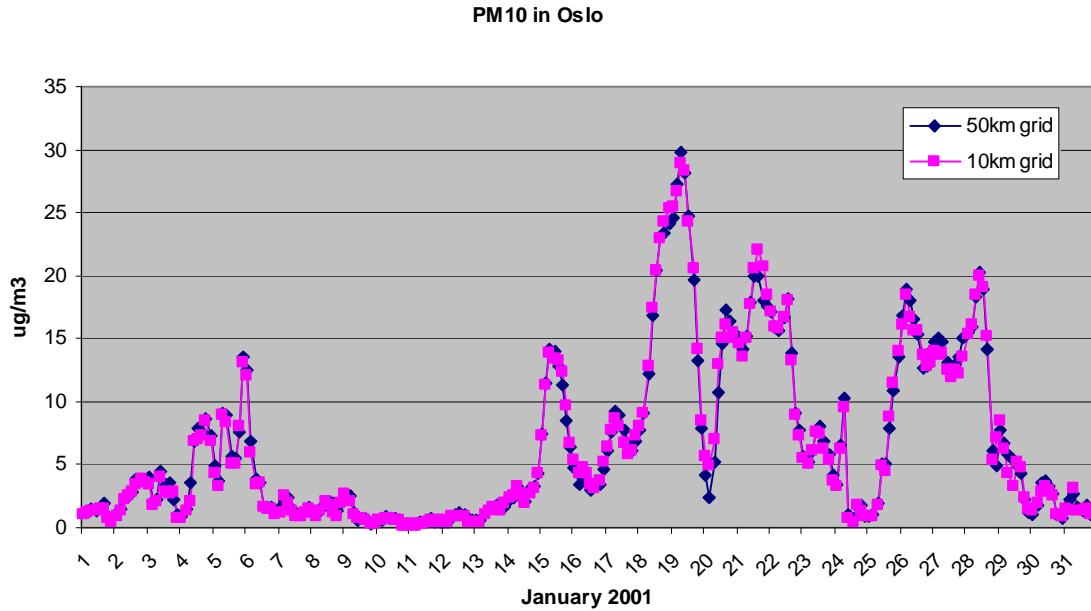


Figure 2.5: Evolution of the PM10 concentrations ($\mu\text{g}/\text{m}^3$) in Oslo simulated in two different grids. The values obtained directly in the 50 km grid are compared with the results obtained in a nested grid with 10 km resolution.

For O_3 and PM10 there are almost no differences between the two simulations. For NO_2 the results are still very similar, but we can observe that several of the highest peaks have different magnitude. More testing will be needed to explain these discrepancies. One possible explanation could lay in the finite rate of updates of the boundary concentrations (three-hourly). Other possibilities could be the differences in timesteps used in the two simulations, or effects of the finer topography used in the construction of the fine grid meteorological data.

Nevertheless, the results are very close for the two simulations. This is an encouraging result. Firstly it shows that the nested model is operational and that it is possible to run consistently the model in different scales. Secondly it demonstrates the ability of the system to test the sensitivity of the concentrations to different input data. By systematically varying the values of the input parameters, the system will give a good measure of the influence of each parameter. This will be the purpose of the experiments documented in the following sections.

2.3.2 Effect of boundary conditions

In the EMEP nesting system, all the information from the regions outside of the grid are transmitted to the grid through the boundary concentrations. The boundary conditions should therefore reflect the effect of long transported pollutants in our simulation. In this section, the sensitivity of the results to the boundary concentrations is measured through the following experiment.

As before the concentrations in Oslo are calculated using a small ($1000 \times 1000 \text{ km}^2$) grid with 10 km resolution nested into the larger grid. A second run is performed in the same small grid, but *without* nesting the small grid into the larger grid. In practice this means that the concentrations at the lateral boundaries are “frozen” at their initial values (which are set to the

default EMEP background concentrations). Since the second run does not contain any input from the larger grid, all the differences must be due to components entering the area through the boundaries. By comparing the results obtained, a first estimate of the effects of updating the boundary concentrations can be provided.

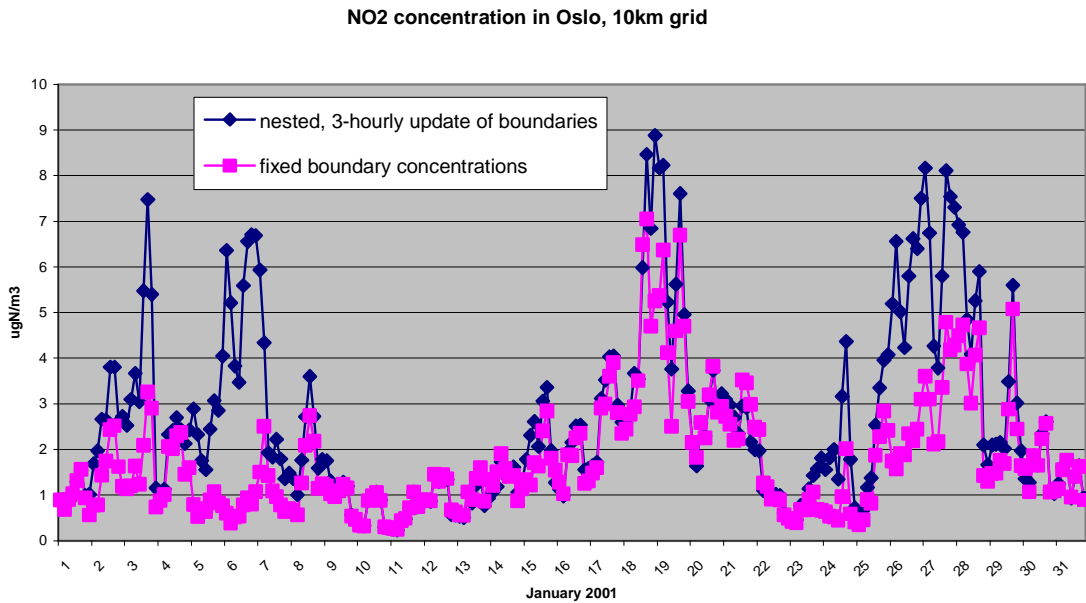


Figure 2.6: Evolution of the NO₂ concentrations ($\mu\text{gN}/\text{m}^3$) in Oslo simulated with two different boundary conditions. In the first case the inner grid is nested with a three-hourly update of the boundary concentrations, and in the second case the boundary concentrations are left unchanged during the run.

In figures 2.6, 2.7 and 2.8 the concentrations of NO₂, O₃ and PM₁₀ obtained with a nested grid are compared with the same calculation performed without nesting the grid (frozen boundary conditions).

Many of the peaks obtained in the nested model runs are not present when the boundaries are frozen. This demonstrates the importance of a correct description of boundary concentrations. The choice of the rate of update will depend on the lifetime of the chemical components and the application of interest.

Note that the fine grid covers in this case a relatively large area around Oslo (500 km on each side). If the fine grid would have been smaller the relative contributions from the outer boundaries would have been even larger.

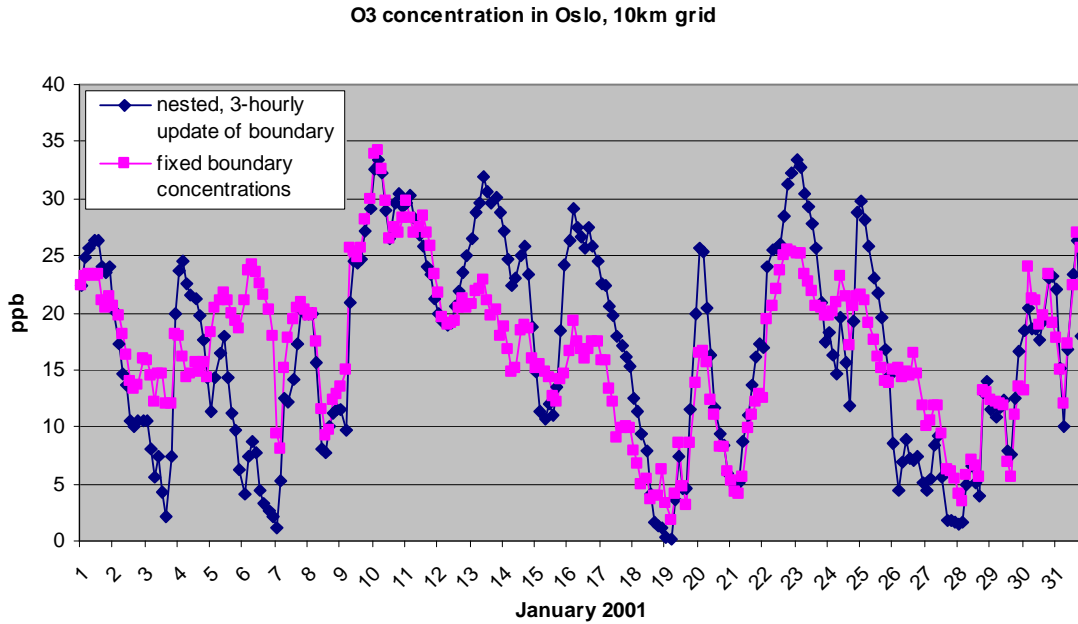


Figure 2.7: Evolution of the O_3 concentrations (ppb) in Oslo simulated with two different boundary conditions. In the first case the inner grid is nested with a three-hourly update of the boundary concentrations, and in the second case the boundary concentrations are left unchanged during the run.

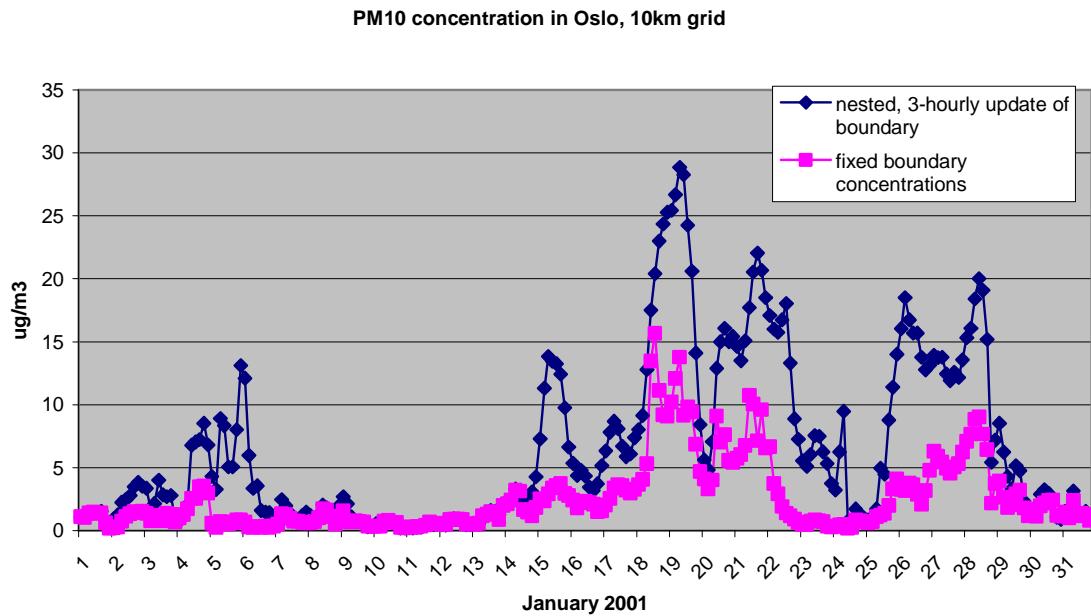


Figure 2.8: Evolution of the PM_{10} concentrations ($\mu g/m^3$) in Oslo simulated with two different boundary conditions. In the first case the inner grid is nested with a three-hourly update of the boundary concentrations, and in the second case the boundary concentrations are left unchanged during the run.

2.3.3 Effect of refined description of emissions

In order to study the sensitivity to refined emission information, two simulations are compared using different sets of emission data in different grid resolutions. To be meaningful the emissions in the fine grid should be realistic and therefore can not simply be interpolated from a coarser grid. Since this information is at present not available for Oslo, we performed the simulations in the region around Berlin, where good quality emission inventories are available (CityDelta).

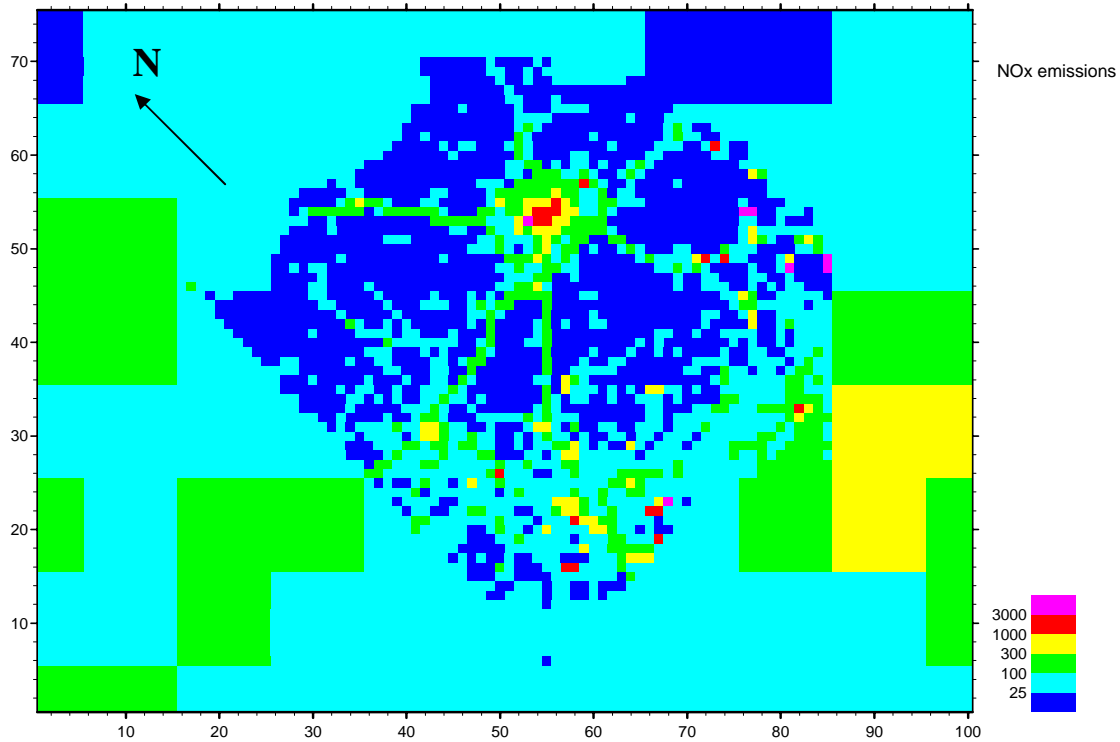


Figure 2.9: *Level of NO_x emissions in the Berlin area in the fine 5x5km² resolution. The city centre and the incoming main roads are clearly visible. In the areas where the emissions are not available in fine resolution, the EMEP emissions in coarse resolution are used. Units: tons (NO₂) per year.*

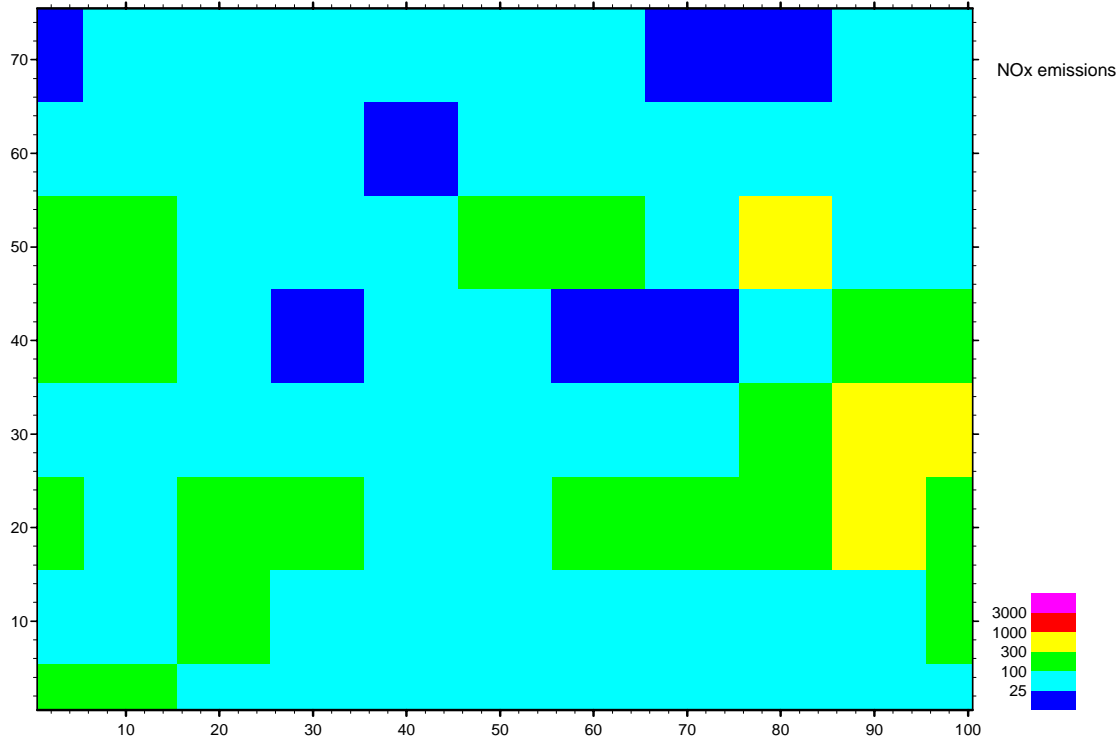


Figure 2.10: Level of NO_x emissions in the Berlin obtained by first aggregating the emissions to the coarse EMEP grid with $50 \times 50 \text{ km}^2$ resolution, and then subdividing each $50 \times 50 \text{ km}^2$ gridcell into 100 small $5 \times 5 \text{ km}^2$ gridcells. The total emissions per $50 \times 50 \text{ km}^2$ gridcell is the same as in figure 2.9, but all the fine structure is smoothed out. Units: tons (NO_2) per year.

For this experiment three sets of emissions are prepared:

- In the first set the fine CityDelta emissions in the Berlin area are distributed in a grid with $5 \times 5 \text{ km}^2$ resolution. Since only two types of emissions are reported in CityDelta (“Ground” and “High”), these are distributed between the different sectors according to EMEP 1999 emissions. In the area where the emissions are not available in the fine resolution, the emissions are completed by EMEP emissions as shown in figure 2.9 .
- In a second set the emissions are aggregated to the coarse EMEP grid with $50 \times 50 \text{ km}^2$ resolution. Note that, in the Berlin area, these emissions will differ from the official EMEP emissions.
- In the third set the emissions from each $50 \times 50 \text{ km}^2$ gridcell are subdivided into 100 $5 \times 5 \text{ km}^2$ gridcells. The emissions obtained in this last set, are represented in a fine $5 \times 5 \text{ km}^2$ grid, but do not contain more refined spatial information than in the coarse grid (figure 2.10). This set will reproduce the emissions which would be used in the case where only a coarse set of emissions was available.

Each set of emissions is used in one run:

- Run1: fine grid ($5 \times 5 \text{ km}^2$ resolution), detailed emission information (figure 2.9)
- Run2: coarse grid ($50 \times 50 \text{ km}^2$ resolution), coarse emission information
- Run3: fine grid ($5 \times 5 \text{ km}^2$ resolution), coarse emission information (figure 2.10)

Run2 is covering the large EMEP grid and is used only to provide the boundary concentrations for the two other simulations. Run1 and Run3 can easily be compared, because the two simulations differ only by the level of refinement in the description of emissions: the size (100×75), the resolution of the grids ($5 \times 5 \text{ km}^2$) and the meteorological input (interpolated from 50 km) are exactly the same.

It would also have been possible to compare Run1 with Run2 instead of Run3, but the results would have been more difficult to interpret, since the effect of refined emissions would be superposed to the numerical effects of the nesting. Although, as shown in section 2.3.1, the numerical effects of the nesting are small.

In figure 2.11 and 2.12 the instantaneous concentrations of NO_2 (on January the 6th at 18:00) are depicted, using the fine and coarse emission sets (Run1 and Run3 respectively).

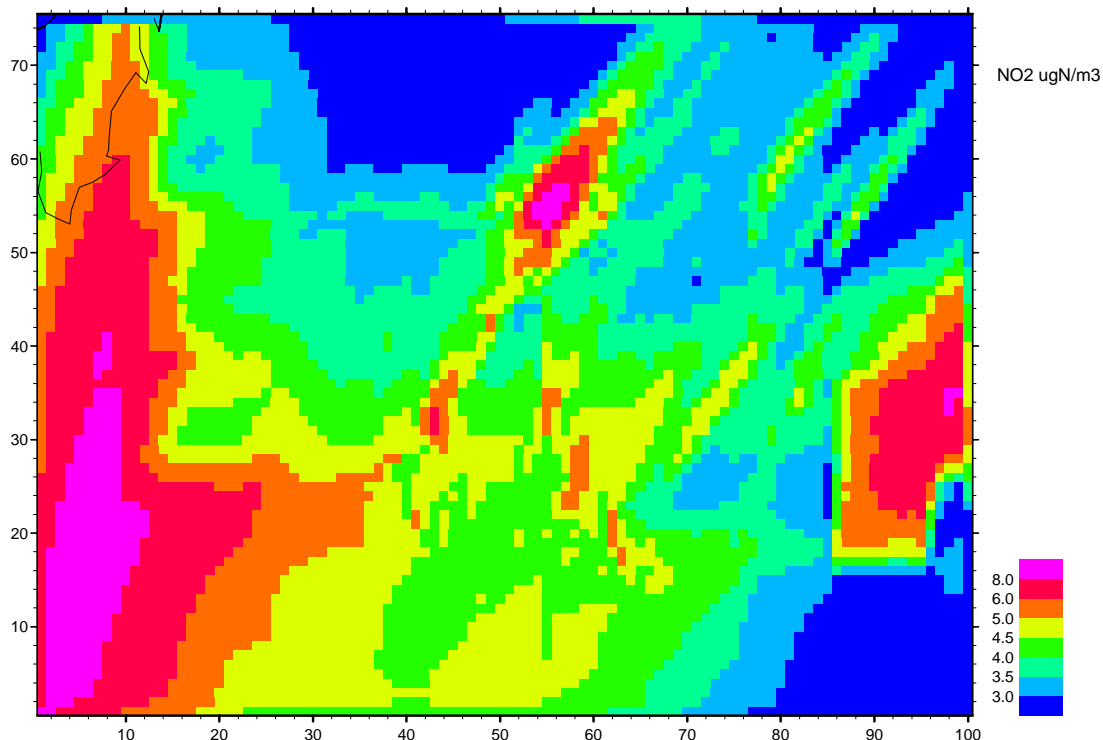


Figure 2.11: Distribution of the instantaneous NO_2 concentration in the Berlin area ($\mu\text{gN/m}^3$) on January the 18th 2001. The concentrations are calculated using a nested $5 \times 5 \text{ km}^2$ resolution grid with the refined emissions (figure 2.9).

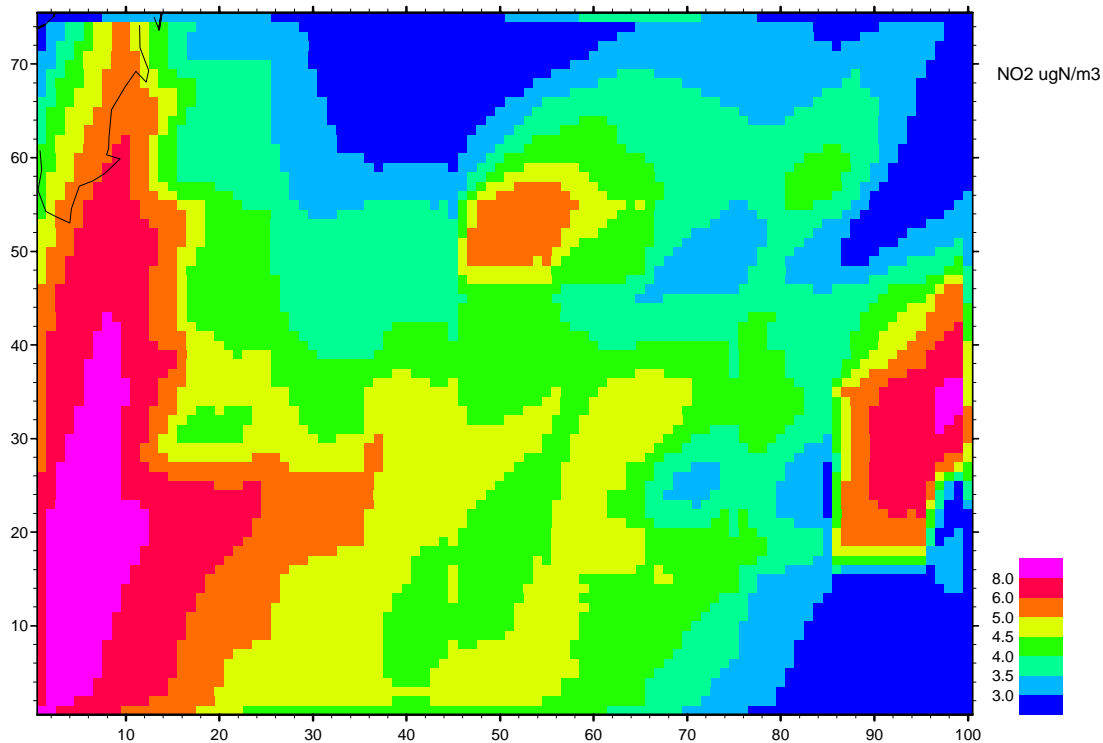


Figure 2.12: Distribution of the instantaneous NO_2 concentration in the Berlin area ($\mu\text{gN}/\text{m}^3$) on January the 18th 2001. The concentrations are calculated using a nested $5 \times 5 \text{ km}^2$ resolution grid and a coarse description of emissions (figure 2.10).

It is interesting to observe that the NO_2 concentrations in figure 2.11 do not reflect all the fine structure present in the emissions (figure 2.9). Only the largest emissions sources create significant peaks. Compared with the figure obtained using coarse emission description (figure 2.12), the concentration levels in the centre of Berlin are much higher in the case where fine emissions are used. However except in the regions very close to large sources the differences are relatively small.

Note also the high concentration levels from pollutants entering the domain through the boundaries (bottom-left on figures 2.11 and 2.12).

A more accurate comparison can be made by comparing the time evolution of the concentrations at different positions. In the next figures (2.13-2.18) the concentrations of NO_2 , O_3 and PM_{10} are plotted at two different positions: at the centre of Berlin (coordinates 55,53 on the figures) and about 41 km East of city centre (coordinates 60,60 on the figures).

The NO_2 concentrations in Berlin calculated with the fine emissions have a much higher level than the concentrations calculated with coarse emissions (figure 2.13). For O_3 the

concentrations are lower in the first case (figure 2.14). For PM10 the concentrations are rather similar in the two situations, but several sharp supplementary peaks are present in the case of fine emissions (figure 2.15). This shows that in the city centre, a significant improvement of the description is reached by using emissions described in a fine $5 \times 5 \text{ km}^2$ resolution.

For the concentrations obtained outside the city centre, the comparison between the two types of emissions shows much less differences than within the city. For NO_2 and O_3 there are only a few episodes (14th, 25th and 29th of January) where the results differ significantly (see figure 2.16 and 2.17). For PM10 there is a noticeable difference only around the 30th of January.

This shows that the difference one can expect by improving the description of emissions, is largely dependent on the distance to strong concentrated sources. The improvement in the description of air pollution levels one can expect from a more refined description of the emissions is rapidly decreasing with the distance to the sources. The relation between the level and distance of emission sources, and the resolution of the grid which is required needs to be further investigated.

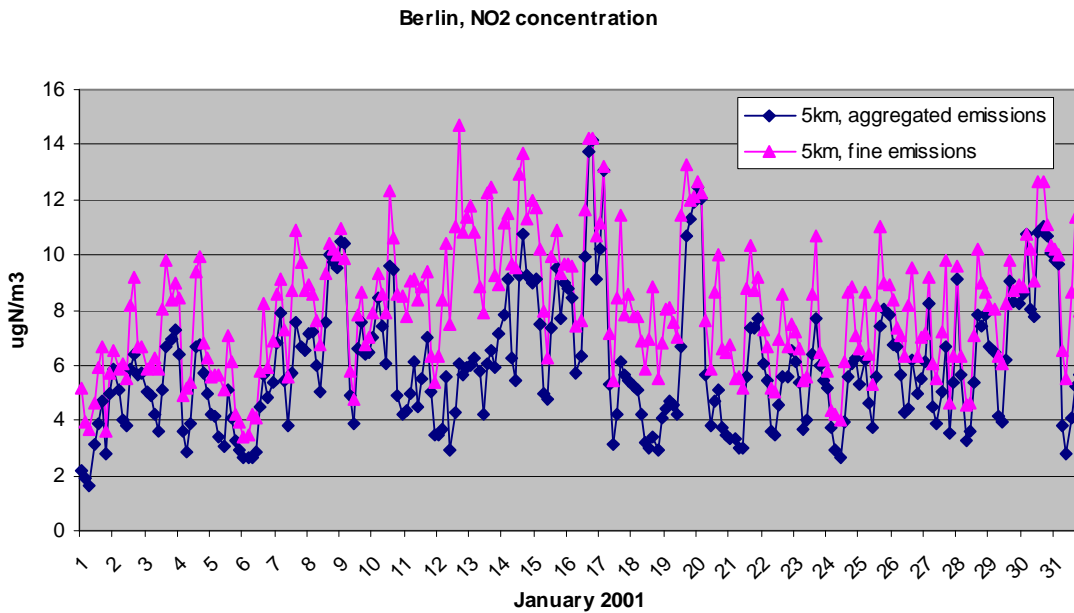


Figure 2.13: Evolution of the NO_2 concentrations ($\mu\text{gN}/\text{m}^3$) in the city of Berlin simulated with two different set of emissions. In the first case the concentrations are calculated using a nested $5 \times 5 \text{ km}^2$ resolution grid and a coarse description of emissions (figure 2.10) and in the second case the refined emissions are used (figure 2.9)

Berlin, O₃ concentration

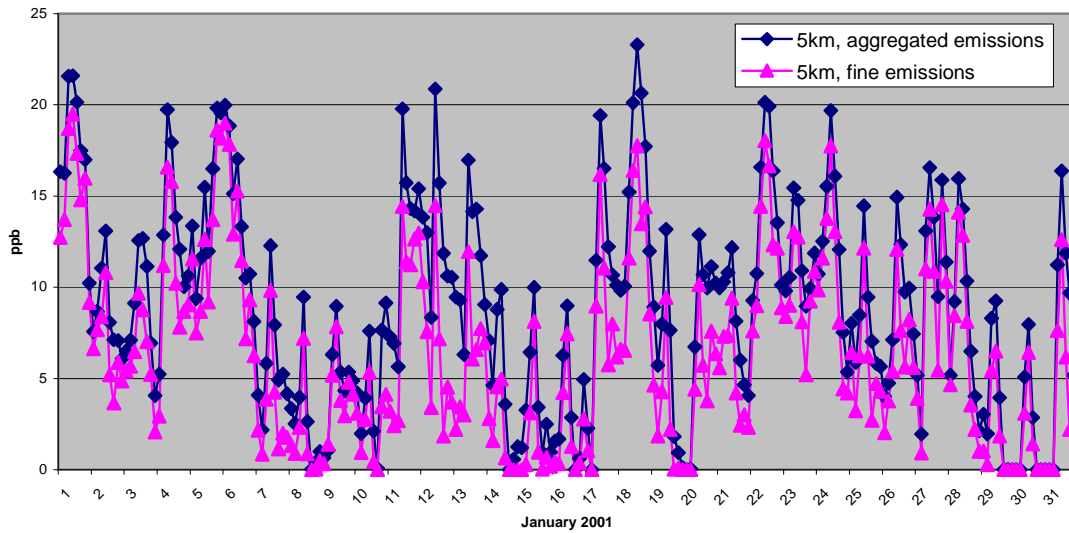


Figure 2.14: Evolution of the O₃ concentrations (ppb) in the city of Berlin simulated with two different set of emissions. In the first case the concentrations are calculated using a nested 5x5 km² resolution grid and a coarse description of emissions (figure 2.10) and in the second case the refined emissions are used (figure 2.9)

Berlin, PM10 concentration

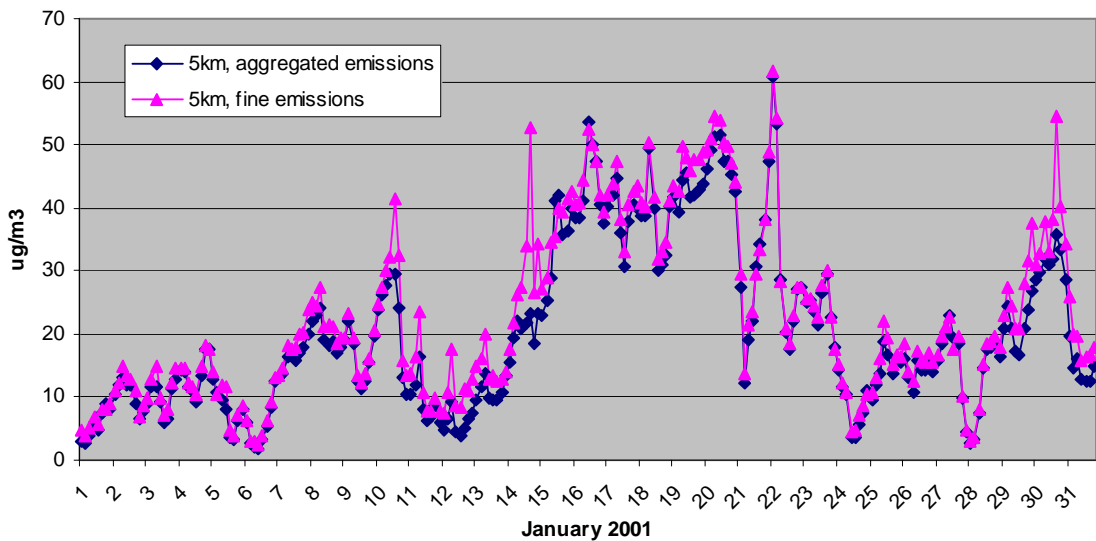


Figure 2.15: Evolution of the PM10 concentrations ($\mu\text{g}/\text{m}^3$) in the city of Berlin simulated with two different set of emissions. In the first case the concentrations are calculated using a nested 5x5 km² resolution grid and a coarse description of emissions (figure 2.10) and in the second case the refined emissions are used (figure 2.9)

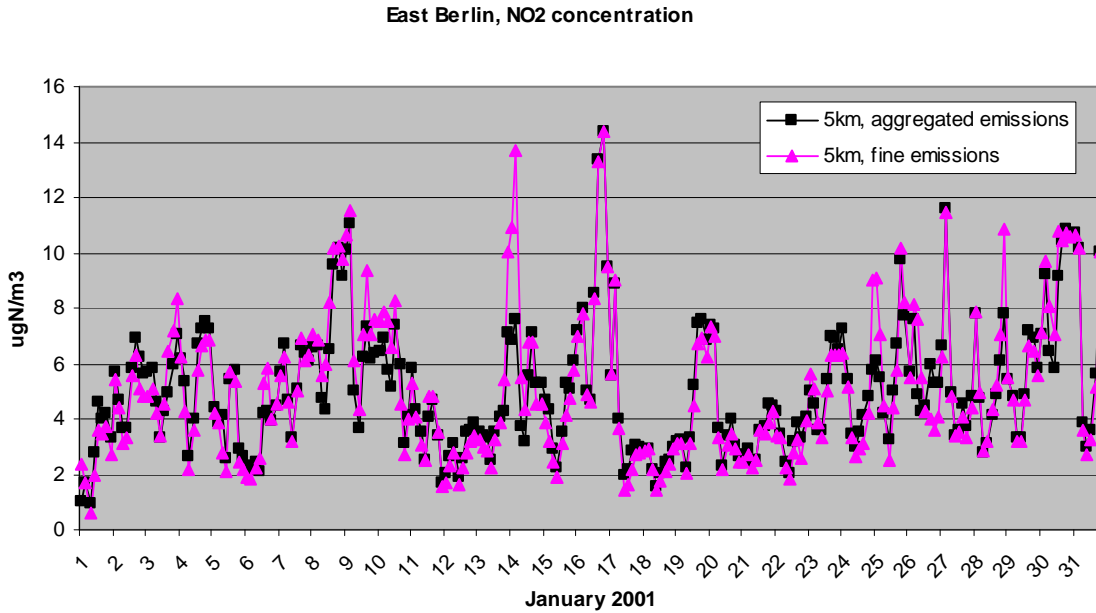


Figure 2.16: Evolution of the NO_2 concentrations ($\mu gN/m^3$) close to Berlin, outside the city centre, simulated with two different set of emissions. In the first case the concentrations are calculated using a nested $5 \times 5 \text{ km}^2$ resolution grid and a coarse description of emissions (figure 2.10) and in the second case the refined emissions are used (figure 2.9)

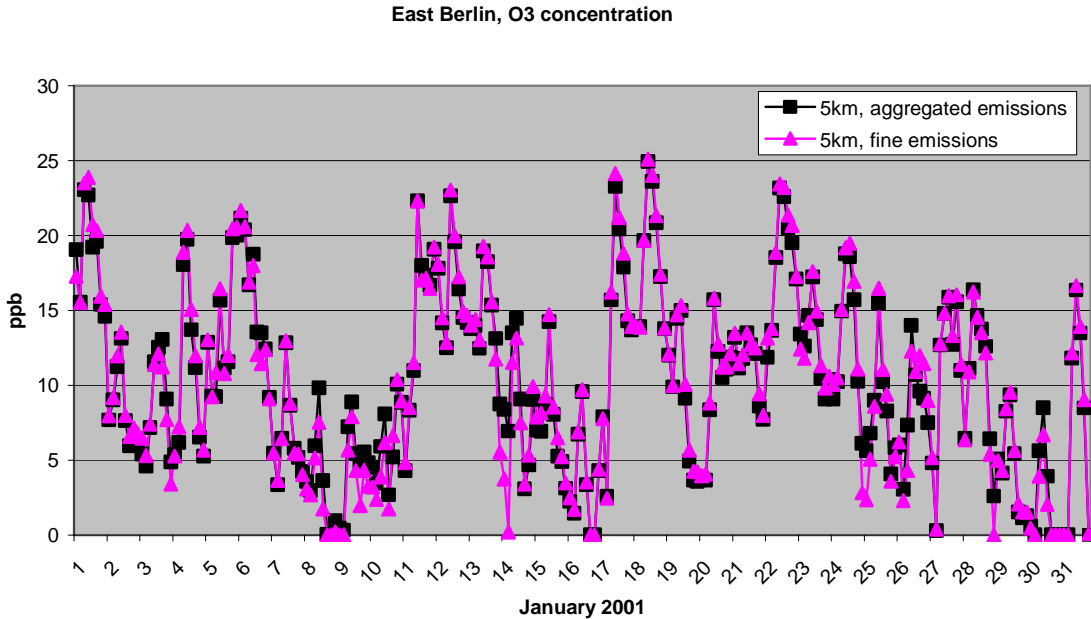


Figure 2.17: Evolution of the O_3 concentrations (ppb) close to Berlin, outside the city centre, simulated with two different set of emissions. In the first case the concentrations are calculated using a nested $5 \times 5 \text{ km}^2$ resolution grid and a coarse description of emissions (figure 2.10) and in the second case the refined emissions are used (figure 2.9)

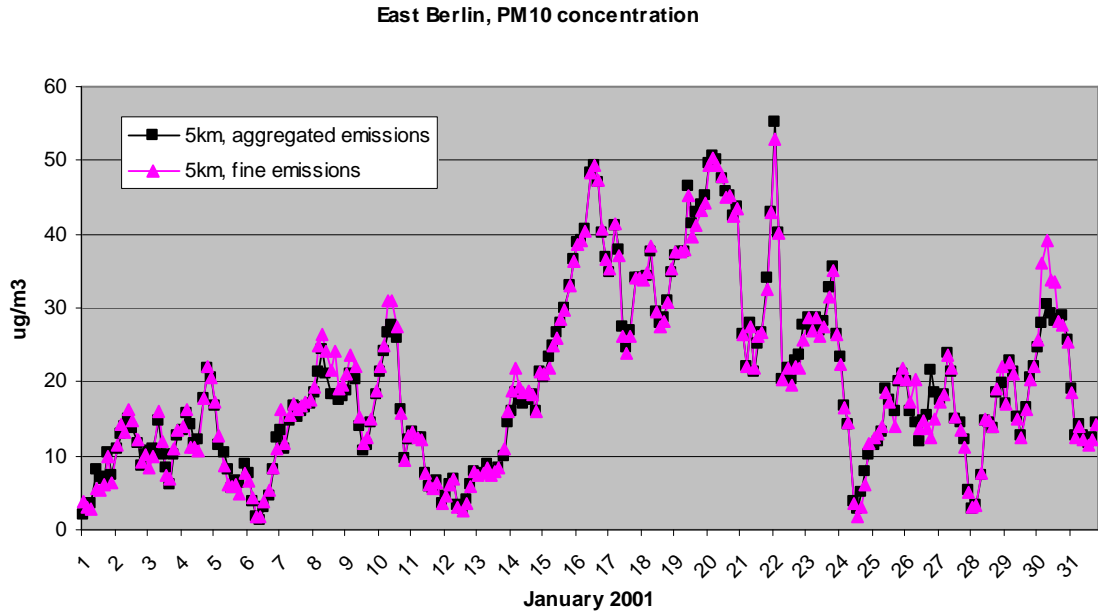


Figure 2.18: Evolution of the PM10 concentrations ($\mu\text{g}/\text{m}^3$) close to Berlin, outside the city centre, simulated with two different set of emissions. In the first case the concentrations are calculated using a nested $5 \times 5 \text{ km}^2$ resolution grid and a coarse description of emissions (figure 2.10) and in the second case the refined emissions are used (figure 2.9)

3. Model development of the urban scale dispersion model EPISODE

Based on the theoretical work performed in phase one of this project (Wind et al., 2002) the following features have now been implemented and tested in the EPISODE model:

- 1) The model code has been reformulated to allow for a new vertical coordinate. The new vertical coordinate is more similar to the coordinate applied in the EMEP model, and therefore better suited for the nesting of the models.
- 2) A new simplified chemistry scheme for photo-oxidants has been implemented. The new simplified scheme considers 45 different species, as compared to more than 70 in the original EMEP chemistry scheme.
- 3) The model has been modified so as to allow for self nesting. This means that the model can be run on successively smaller sub-domains with increasing model resolution. In this sequence of model simulations the necessary boundary conditions for each sub-domain are produced by the previous (coarser) model run.
- 4) Conversion routines have been produced so as to allow for fully coupled model simulations, in which the boundary conditions for the outer EPISODE domain have been produced by the EMEP Unified Model. Since the necessary emission data for a realistic photo-oxidant simulation only have been available for a model area covering the city of Berlin, this area has been chosen as a demonstration site for the fully coupled EMEP/EPISODE model system.

As a result of the above achievements the EPISODE model can now be applied for one-way nested, photo-chemical (45 components including O₃/NO₂) simulations. Computed boundary conditions produced by the EMEP Unified Model can be applied at the open boundaries of the outermost EPISODE model domain, and then the boundary conditions for the subsequent self nested model domains are produced internally by EPISODE.

3.1 Implementation of the new vertical coordinate transform in EPISODE

The new vertical coordinate transform proposed for EPISODE in phase one of this project (Wind et al., 2002) has now been implemented in the model code. The applied transform is identical to the one described in Wind et al., 2002, but a slight change in notation has been made, resulting in a minor change in the resulting equations. Because of this a brief description of the new coordinate transform and the resulting model equations are presented below.

The new terrain following sigma-z coordinate system implemented in EPISODE is now defined by the transformation:

$$\sigma = \sigma(x, y, z) = H_0 \frac{z - h(x, y)}{H_0 - h(x, y)}. \quad (1)$$

Here z denotes the Cartesian height, $h(x,y)$ is the terrain height, and H_0 is a constant height defining the top boundary of the model domain. All of these heights are specified in meters and are measured from a common reference level. Note that the denominator of (1) is identical to the total vertical depth of the model, i.e. $D(x,y)$ defined as:

$$D(x,y) \equiv H_0 - h(x,y) \quad \Leftrightarrow \quad h(x,y) = H_0 - D(x,y).$$

From (1) it is seen that $\sigma = 0$ at the ground, i.e. for $z = h(x,y)$, and $\sigma = H_0 = \text{const.}$ at the model top boundary, i.e. for $z = H_0$.

In this transformed coordinate system, and with the additional assumptions of an incompressible wind field (e.g. a divergence-free wind field), and of a simplified parameterisation of the terms describing the horizontal turbulent diffusion (Wind et al., 2002), the resulting advection/-diffusion equation in EPISODE becomes

$$\begin{aligned} \frac{\partial c_i}{\partial t} + \frac{1}{D} \left(\frac{\partial(u c_i D)}{\partial x} + \frac{\partial(v c_i D)}{\partial y} + \frac{\partial(\omega c_i D)}{\partial \sigma} \right) = \frac{\partial}{\partial x} \left(K^{(H)} \frac{\partial c_i}{\partial x} \right) + \frac{\partial}{\partial y} \left(K^{(H)} \frac{\partial c_i}{\partial y} \right) + \\ \left(\frac{H_0}{D} \right)^2 \frac{\partial}{\partial \sigma} \left(K^{(Z)} \frac{\partial c_i}{\partial \sigma} \right) + R_i - S_i. \end{aligned} \quad (2)$$

The new vertical velocity, ω , is defined by

$$\omega \equiv \frac{H_0}{D} w - (H_0 - \sigma) \frac{u}{D} \frac{\partial h}{\partial x} - (H_0 - \sigma) \frac{v}{D} \frac{\partial h}{\partial y}, \quad (3)$$

and the incompressible wind field satisfy the continuity equation

$$\frac{\partial(uD)}{\partial x} + \frac{\partial(vD)}{\partial y} + \frac{\partial(\omega D)}{\partial \sigma} = 0. \quad (4)$$

The above equations differ slightly from the corresponding equations in Section 4.1.4. of Wind et al. (2002), as a result of a small modification of the definition of the new vertical velocity, ω . This modification has only been made in order to comply with commonly used notation, and it has no practical influence on the model performance.

The implementation of the new vertical coordinate system in EPISODE has mainly affected the numerical algorithms describing the horizontal and vertical advection, the vertical turbulent diffusion, and the diagnostic expression of the new vertical velocity, ω .

3.2 Photochemical mechanism in the EPISODE model

The aim of this part of the project was to extend the chemistry in the EPISODE model from the previous photochemical steady state assumption to a routine that is able to calculate photochemical reactions.

3.2.1. The present chemical routine in EPISODE

Presently EPISODE uses the photostationary state assumption that is based on an instantaneous equilibrium between the following three reactions:



The steady-state assumption implies that NO_x (the sum of nitrogen oxides) and O_x (oxidants) are conserved, where NO_x and O_x are defined as:

$$[\text{NO}_x] = [\text{NO}] + [\text{NO}_2] , \quad \text{and} \quad [\text{O}_x] = [\text{O}_3] + [\text{NO}_2] .$$

By these assumptions the three components NO, NO_2 and O_3 could be found by the solution of a second-degree equation in O_3 .

This is a valid assumption in urban areas from a short distance away from the emissions until a net ozone formation is starting. In polluted areas in the north in winter this will be a good assumption. However, when the solar UV-radiation is stronger, either because of a more southern location or in summer, a net ozone formation could take place even in urban areas a certain distance away from the main emission sources. Thus, the assumption of conservation of O_x and NO_x is then not valid and a more detailed chemical description is needed.

The change from a photostationary steady state assumption to a chemical routine able to simulate net ozone formation requires integration of a system of partial differential equations for a number of components.

The following explains the work from a literature study of chemical codes presently available, through an evaluation of these to a preparation of a compact chemical scheme and a final testing of the procedure in the EPISODE model.

3.2.2 Evaluation of chemical mechanisms available

A wide range of photochemical mechanisms and models are applied today, from extremely detailed and comprehensive codes including thousands of reactions (the Master Chemical Mechanism) down to highly simplified, so-called "lumped", mechanisms. A lumped chemistry implies that the calculations are carried out only for a small group of selected species that are meant to be representative for the thousands of organic species actually involved.

Obviously, for a 3D CTM like EPISODE, to be run on a PC platform, the mechanism and number of compounds has to be reduced to a minimum. A literature study was carried out and a number of available chemical schemes were identified. Table 1 gives an overview of chemistry codes easily accessible and applied in various models.

Table 1.

	No. of species	No. of reactions	Used by	Variations
EMEP	68	140	EMEP	
CBM-IV	32	81	UAM ROM LOTOS	CBM-IV-LOTOS CB4-TNO CBM-IV-99
SAPRC	~54	~158	CALGRID REM3	SAPRC-90, -93, -97, -99
RADM	55	156	RADM (EPA) EURAD	RADM2 RACM (69 spec.) ReLACS (37 spec.)
ADOM	47	114	ADOM	
UiB	51	111	Univ. of Bergen	

CBM-IV developed by the Environmental Protection Agency, EPA, as well as SAPRC and RADM are all American codes widely applied in photochemical models. The compact CBM-IV mechanism is however not easily compatible with e.g. the EMEP mechanism as the type of chemical lumping differs substantially. Thus, it was concluded that a simplified version of the EMEP chemical routine would be preferable in this work.

3.2.3 Simplifications of the EMEP mechanism

The EMEP chemistry is designed for calculating photochemical reactions on a regional, European scale, covering all kinds of environments from clean, background conditions to polluted semi-urban areas and time scales of several days. For EPISODE, the requirements are significantly lower – the model will be applied for more polluted regions and the residence time of the atmospheric species will normally be limited to less than a day.

Given these conditions, the chemistry implemented in EPISODE could be simplified while still being compatible with the EMEP model. Such simplifications would, however, be redundant if CPU-time and memory were unimportant quantities.

Two main simplifications were done:

1) *RO₂ + RO₂ reactions were omitted*

It is well established that RO₂ in the main ozone formation reaction:



competes with the self-reaction(s)

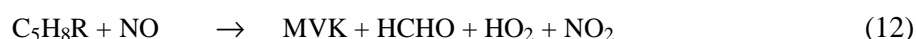


R stands for an organic fraction, and RO₂ denotes a peroxy radical. In low-NO_x environments (NO < 50 pptv) the rates of reaction (9) and (10) will be similar or faster than reaction (8), whereas at NO_x -levels typical of moderately (or more) polluted areas, reactions (9) and (10) will be negligible compared with reaction (8). Thus, all reactions of

type (9) and (10) except for the $\text{CH}_3\text{O}_2 + \text{HO}_2$ and the $\text{HO}_2 + \text{HO}_2$ reactions were omitted from the simplified EMEP scheme.

2) Simple isoprene mechanism

The isoprene mechanism presently included in the EMEP chemistry (Simpson, 1995) is fairly extensive and was significantly simplified in the EPISODE mechanism. Reactions (11) – (14) below show the reduced 4-reactions isoprene scheme used.



where MVK stands for methyl vinyl ketone.

With these two types of simplifications a condensed EMEP mechanism with the number of components reduced from 70 to 45 and the number of reactions reduced from about 150 to about 70 was obtained.

Note that dry deposition is included in the chemistry scheme but wet-scavenging is not.

3.2.4 Numerical implementation of the new chemical scheme in EPISODE

The atmospheric photochemistry equations defined by the condensed mechanism described in sections 3.2.1-3 forms a stiff non-linear system of ordinary differential equations (stiff ODE):

$$\frac{dy}{dt} = f(t, y) = P(t, y) - L(t, y) \cdot y, \quad k = 1, \dots, m. \quad (15)$$

where y is the solution vector containing m components ($m = 45$), and P and L describe the photochemistry production and loss terms respectively. Here $P(t, y)$ is a vector of size m and $L(t, y)$ a diagonal matrix of size $m \cdot m$.

To integrate this system of equations, a new numerical solver has been developed as part of the EPISODE model. The solver is based on the work described in Verwer and Simpson (1995).

First the system of non-linear equations (15) is approximated by a variable-step, second order Backward Differentiation Formula (BDF) formulation:

$$y^{n+1} = Y^n + \gamma \cdot \tau \cdot f(t_{n+1}, y^{n+1}) \quad (16)$$

where $\tau = t_{n+1} - t_n$ is the time step between the solution values y^n and y^{n+1} , and where $\gamma = (c+1)/(c+2)$, $c = (t_n - t_{n-1})/(t_{n+1} - t_n)$ and $Y^n = ((c+1)^2 y^n - y^{n-1}) / (c^2 + 2c)$.

By exploiting the chemical kinetics form of the differential equation (15), where P and L are the production and loss terms respectively, the non-linear system of equations (16) can be written:

$$y_k^{n+1} = \frac{Y_k^n + \gamma \cdot \tau \cdot P_k(t_{n+1}, y^{n+1})}{1 + \gamma \cdot \tau \cdot L_k(t_{n+1}, y^{n+1})} = F_k(y^{n+1}), \quad k = 1, 2, \dots, m. \quad (17)$$

A Gauss-Seidel iteration technique is then employed in order to solve (17) numerically for y^{n+1} , given the values y^n and y^{n-1} at the two previous time steps t_n and t_{n-1} .

As initial iterate we use the following extrapolation formula:

$$y^{(0)} = y^n + \frac{1}{c}(y^n - y^{n-1}) \quad (18)$$

which is the same as described in Verwer and Simpson (1995). A prescribed number of iterations of the Gauss-Seidel technique is then used in order to give an approximate solution to (17). As shown in Verwer and Simpson (1995), a Gauss-Seidel iterative method on the type of photochemistry schemes employed here converges rapidly, so only a small number of iterations are usually required. In their paper they found that 2 iterations were most often enough, and consequently, we have also used 2 iterations per time step.

In order to retain accuracy of the solution of the stiff ODE, a local error indicator is used:

$$E^{n+1} = \frac{2}{c(c+1)}(cy^{n+1} - (1+c)y^n + y^{n-1}) \quad (19)$$

Based on this local error indicator vector, we calculate the weighted error norm:

$$\|E^{n+1}\|_w = \max \left(\frac{|E_k^{n+1}|}{W_k^n} \right), \quad W_k^n = \text{atol}_k + \text{rtol}_k \cdot |y_k^n| \quad (20)$$

where atol_k and rtol_k for $k = 1, \dots, m$, are the component-wise defined absolute and relative error tolerances. If $\|E^{n+1}\|_w \leq 1.0$, the integration step is accepted. Otherwise it is rejected. The new time step, τ_{new} , is estimated by the common formula:

$$\tau_{\text{new}} = \max \left(0.5, \min \left(2.0, \frac{0.8}{\sqrt{\|E^{n+1}\|_w}} \right) \right) \cdot \tau_{\text{old}} \quad (21)$$

where τ_{old} is the previous time step. In our implementation the relative error tolerance is currently set equal to 0,1 (10% relative error) for all components. The absolute error tolerances are set in the range between $2,5E+8$ molec/cm³ and $1,0E+15$ molec/cm³ depending on component.

The step size is further constrained by a prescribed minimum and maximum value. Currently the minimum step size is set equal to 0,1 s and the maximum step size is set equal to two times the step size used in the EPISODE model.

If two successive rejections occur the process is restarted. The missing starting value after a restart, or at the beginning of the simulation period, is calculated by the implicit Euler method:

$$y_k^{n+1} = \frac{y_k^n + \tau \cdot P_k(t_{n+1}, y^{n+1})}{1 + \tau \cdot L_k(t_{n+1}, y^{n+1})}, \quad k = 1, 2, \dots, m. \quad (22)$$

which is treated with the Gauss-Seidel iterative method in the same way as the second order BDF equation. In this case the initial step size is computed by replacing E^{n+1} in (20) with $\tau \cdot f(t_0, y^0)$. Hence we define τ such that the weighted error norm is equal to one, i.e.,

$$\tau = \min \left(\frac{W_k^0}{|f_k(t_0, y^0)|} \right), \quad k = 1, 2, \dots, m. \quad (23)$$

The second order BDF scheme is then applied with the same step size, and after that the variable step size mechanism is again activated. Normally (23) leads to a rather small initial guess for the time step which will be accepted, and then subsequently increased according to (21).

The above described photochemistry operator (numerical solver) is used alternately with the different transport (advection and diffusion) operators in the EPISODE model for every time step t in the model in the following fashion:

$$\text{TRANSPORT}(t) \Rightarrow \text{PHOTO}(2t) \Rightarrow \text{TRANSPORT}(t)$$

where $\text{TRANSPORT}(t)$ is the total transport operator which includes all the horizontal and vertical advection and diffusion operators, and $\text{PHOTO}(2t)$ is the photochemistry operator (numerical solver) as described above, working over a total time span of $2t$. Each time PHOTO is started between the transport operators it is considered as a restart of the method, and thus the implicit Euler method is invoked with an initial time step calculated by (23).

All reaction rate constants were revised and updated according to the most recent edition published by IUPAC (IUPAC, 2001).

The simplified chemistry scheme has been applied in real case simulations for the city of Berlin, see Chapter 4 below for a more detailed description of these simulations. The scheme seems to behave reasonably, and rather good agreement has been found both with local measurements and with model results from other Chemical Transport Models. These EPISODE calculations, considering 45 different species, have been run on an ordinary 2 GHz PC within an acceptable amount of time, i.e. about 6 CPU-hours for a one month calculation period.

3.3 Development of a self-nested version of EPISODE

Previous versions of the EPISODE model only applied spatially constant background concentration values at the open boundaries of the model domain. This background value was traditionally estimated from measurements made at regional background stations. However, these stations are typically located quite far away from urban areas and are therefore, for urban model applications, normally not representative for the air masses flowing in through the model boundaries. In addition only a few components are available at the regional background stations, and their time resolution is rather coarse. Moreover, for forecast applications measured boundary values are of course not available. These deficiencies motivated the present effort of changing the model concept so that model generated concentration values in a coarse model grid could be applied as boundary values for a smaller sub-domain with finer grid resolution. The idea is to allow for an automatic flow of information from the coarse grid to the fine grid, thereby obtaining a one-way, self-nesting modelling system.

3.3.1 Summary of the necessary EPISODE changes to allow for self-nesting

A considerable part of the work of the present phase of the project has been devoted to the implementation of the self-nesting capabilities. The following self-nesting procedure has been implemented in the EPISODE model: The model has been changed so that it can read spatially variable boundary values at specified intervals in time. Functionality has also been included so that initial and boundary values are produced for a user defined, nested sub-domain during a model run. The model simulation can then be repeated for the nested sub-domain using the initial and boundary values produced in the previous coarse grid simulation as inputs, and with new boundary values produced for yet another sub-domain, and so on. In this way model results can be calculated for gradually smaller domains, with increasing resolution.

A short description of the different changes that have been implemented in EPISODE in order to facilitate the above nesting functionality is listed below.

- For all of the gridded model variables (e.g. for all of the present 45 air quality components, and the applied meteorological field data) the domain dimensions have been increased to allow for the boundary grid points at the open boundaries.
- The numerical algorithms describing advection and diffusion have been changed so as to allow for the proper influence of the boundary values. In the present version the boundary values are prescribed at both inflow and outflow boundaries (Dirichlet condition). Another possibility is to prescribe the solution only at inflow boundaries and to apply a zero-gradient condition at outflow boundaries, but this method has not yet been implemented in the model.
- The model interface has been changed so that the necessary information about the position, extent, and resolution of the nested sub-domain is properly defined. For the moment the nested domain is required to be a true sub-domain of the coarse model domain. A further restriction is that the two nests must have the same orientation. As long

as these two conditions are met, the size and position of the nested domain can be chosen freely. Even the vertical model extent and the vertical resolution can be different.

- The necessary initial and boundary values for the nested sub-domain are calculated by interpolation of the coarse grid concentration values. Horizontally, a simple bi-linear interpolation method is used. Optionally, a Bessel-interpolation can be applied. If the nested sub-domain has a different vertical resolution than its parent grid, linear interpolation is employed in this direction.
- New import and export routines for the initial and boundary values of the nested domain have been implemented.

3.3.2 Idealized test simulations

Continuing from the idealized experiments performed in phase one of this project (Wind et al., 2002), the self-nested EPISODE version has been tested for a situation in which an analytical (Gaussian) cloud of an inert pollutant has been advected and diffused through both a coarse and a nested model domain. This analytical solution has been applied in order to facilitate quantitative assessments of the errors introduced by the nesting procedure. The non-stationary analytical pollution cloud is defined as

$$C_B(x, y, z, t) = \frac{q}{4(\pi \cdot t)^{3/2} K^{(H)} (K^{(Z)})^{1/2}} \cdot e^{-\frac{[x-x_0-u(t-t_0)]^2 + [y-y_0]^2}{4tK^{(H)}}} \cdot e^{-\frac{z^2}{4tK^{(Z)}}}, \quad (24)$$

where q is the mass of the pollutant cloud, x_0 and y_0 is the position where the mass q was emitted at time t_0 . $K^{(H)}$ and $K^{(Z)}$ are the horizontal and vertical diffusivities, respectively. Expression (24) is a valid solution of the advection/diffusion equation that is solved numerically in EPISODE, i.e. equation (2), as long as the diffusivities are constant, and that the diffusivity in the horizontal is independent on direction. To comply with this the EPISODE model has in these experiments been run with constant diffusivities of $K^{(H)} = 20 \text{ m}^2/\text{s}$ and $K^{(Z)} = 1 \text{ m}^2/\text{s}$. Furthermore, (24) is only valid for instantaneous ground level emissions with no deposition at the ground. Equation (24) is describing a normal (bell-shaped) distribution, and the traditional way of expressing this distribution is found by substituting:

$$\sigma_H = (2K^{(H)}t)^{1/2} \quad \text{and} \quad \sigma_z = (2K^{(Z)}t)^{1/2} \quad (25)$$

where σ_H and σ_z are the standard deviations in the horizontal and vertical direction of the concentration distribution, respectively. This means that 95.45 % of the pollutant mass is found within horizontal distances of $\pm 2 \sigma_H$ from the centre of the bell-shaped function and below the height of $2 \sigma_z$ from ground (68.27 % inside one sigma, 99.73% within 3 sigma). In these tests a constant wind speed of 1 m/s has been applied.

By defining (24) as the boundary solution, and by adjusting x_0 , y_0 , and t_0 accordingly, a cloud of a resolvable size could be specified to enter the coarse model grid through the upwind (western) open boundary. The horizontal resolution of the coarse grid was 3 km, and the computed values within this coarse grid was then applied as boundary conditions for a smaller fine grid sub-domain with a horizontal resolution of 1 km.

The coarse grid (3 km) simulation was run twice. In the first run the analytical boundary solution was updated every time step, i.e. every 5 minutes, and in the second it was just updated once every hour. Under normal circumstances the boundary values will be available for every 1, 3 or 6 hours, depending on the spatial scale of the model domain. In figure 3.1 a cross-section of the calculated coarse grid concentrations in the lowermost model layer are presented for both simulations. The cross-section goes through the maximum value of the bell shaped cloud and is directed along the wind vector. The x-axis indicates the distance measured in grid points from the upwind model boundary. The three curves in the figure show the analytical boundary solution, and the two calculated coarse grid solutions after 24 of simulation.

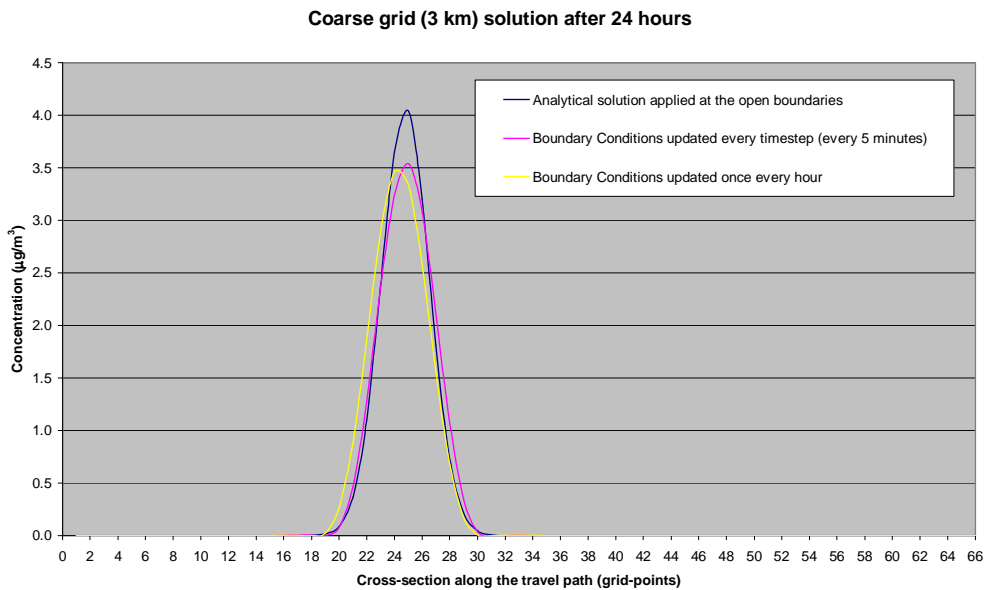


Figure 3.1: A cross-sectional view of the analytical solution and the calculated coarse (3 km) grid concentrations in the lowermost model layer after 24 hours of simulation. The calculated solution is shown both for the case when the boundary values are updated every time step (every 5 minutes) and when they are updated once every hour.

As seen in figure 3.1 there is generally good agreement between the computed and the analytical solutions. The most pronounced difference is that the computed solutions display a lower maximum value than the analytical solution. Based on the test results reported in phase one of this project (Wind et al., 2002) this effect is assumed to be caused by too low resolution. The solution with boundary updating every time step is slightly advancing the analytical solution, while the hourly updated solution lags somewhat behind. Note that larger differences between the two computed solutions are to be expected for increasing wind speeds since the applied time step will be less than 5 minutes in this case.

In figure 3.2a and 3.2b the corresponding cross-section for the nested sub-domain are shown after 24 and 36 hours of simulation, respectively. In this fine grid simulation the boundary values for both simulations are updated once an hour, but the applied boundary values are taken from the two coarse grid simulations with different boundary value updating shown in figure 3.1.

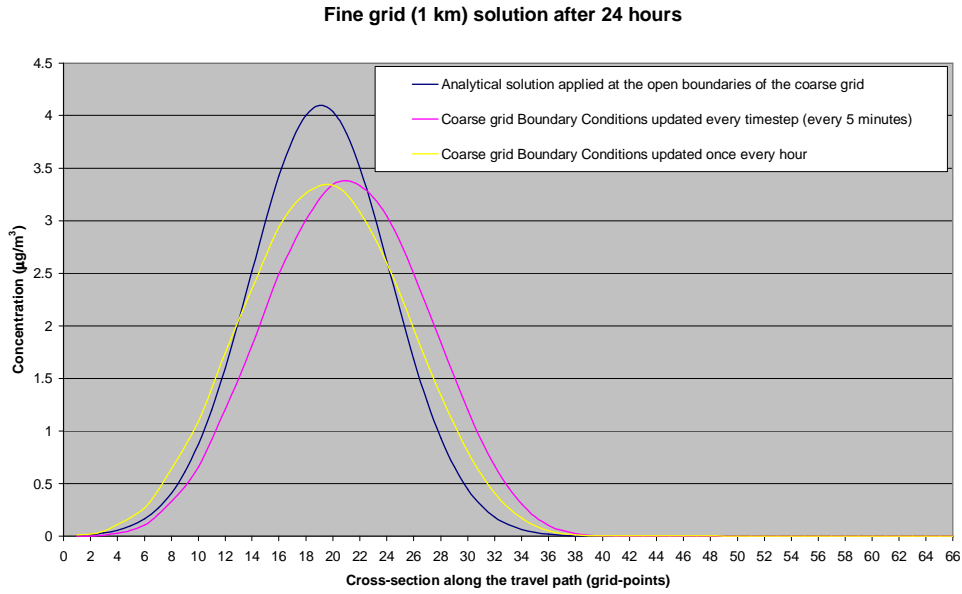


Figure 3.2a: A cross-sectional view of the analytical solution and the calculated fine (1 km) grid concentrations in the lowermost model layer after 24 hours of simulation. The calculated solution is shown both for the case when the boundary values are updated every time step (every 5 minutes) and when they are updated once an hour.

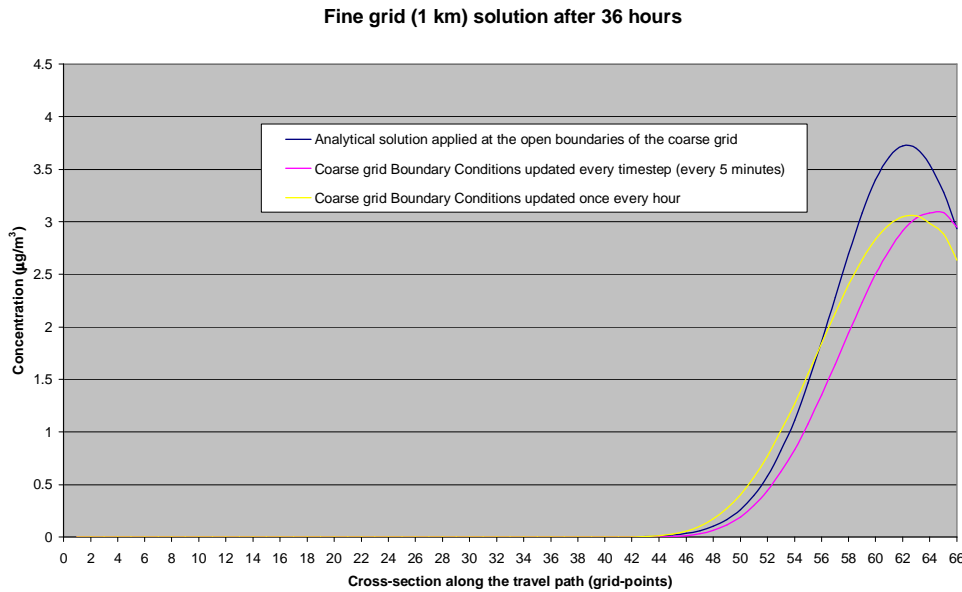


Figure 3.2b: A cross-sectional view of the analytical solution and the calculated fine (1 km) grid concentrations in the lowermost model layer after 36 hours of simulation. The calculated solution is shown both for the case when the boundary values are updated every time step (every 5 minutes) and when they are updated once an hour.

The same general features, as revealed in the coarse grid simulation, are also found in the nested fine grid results. The tendency of a somewhat higher advection speed in the model, combined with the lag caused by the hourly boundary value updating in the coarse grid simulation adds up to an almost perfect match in advection speed for the yellow curve in figure 3.2a and 3.2b. By comparing the curves of the computed solutions after 24 hours of

simulation time, shown in figure 3.1 and 3.2a, it is seen that the nesting procedure only leads to a minor spatial spread of the bell-shaped distribution combined with a slight lowering of the concentration amplitude. In figure 3.2b the solutions are shown as they leave the nested model domain. No severe signs of artificial boundary effects are seen in the computed solutions, indicating that the applied boundary conditions works properly.

A crucial requirement for a one-way nested air quality model is that the pollutant mass is maintained when transported into the nested domain. In order to investigate whether this requirement is fulfilled in our model system the total pollutant mass within each model domain has been calculated for all of the experiments shown in figure 3.1 and 3.2. The resulting total mass time series are presented in figure 3.3 below.

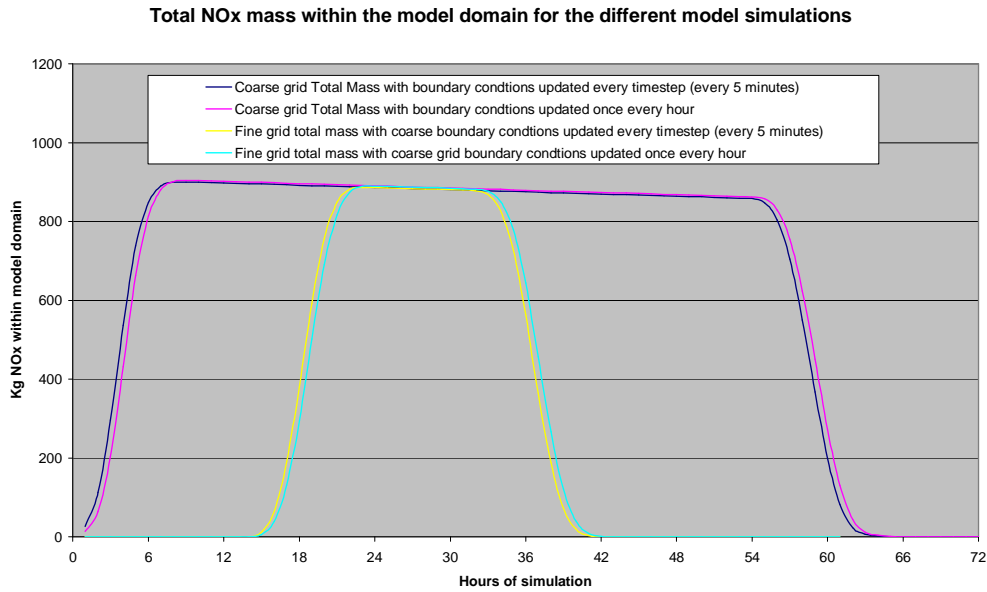


Figure 3.3: Total mass of NOx within the model domain for the four simulations shown in figure 3.2.

The curves in figure 3.3 clearly reveal that the cloud mass enters the nested fine grid domain without any sign of loss in mass. The lagging of the hourly updated solution is also seen in figure 3.3. The slight decrease in model mass during the cloud passage is due to the turbulent diffusive loss through the top boundary of the model domain.

Based on the above results it can be concluded that the one-way nesting procedure presently implemented in EPISODE seems to work properly. Time-dependent and spatially varying concentration fields can be transported from a coarse model domain into a nested sub-domain without significant distortion or loss of pollutant mass.

3.3.3 Test experiments with variable topography for the city of Oslo

More realistic NO_x-simulations for the city of Oslo have also been performed. In these simulations a model domain of 22 km x 18 km centred around the city area, with a 1 km horizontal resolution, has been used as the coarsest grid, with a nested sub-domain of similar grid dimensions with a horizontal resolution of 500 m. The meteorological inputs for these two domains have been produced by use of the diagnostic wind-field model MATHEW (Sherman, 1975; Foster et al., 1995; Slørddal, 2002). Note that the calculations of the wind fields have been performed with topographical data given with a horizontal resolution of 1 km and 500 m in the coarse and the fine domain grid, respectively. This means that the fine grid simulation contains much more topographical detail than the coarse model run, and the computed wind field close to ground may therefore vary significantly both in speed and direction in areas where the topographical features are described differently in the two resolutions.

The main aim of these test-simulations has been to investigate the impact of variable topography when applying a self-nested modelling system. Since it is expected that the wind field can be severely influenced by changes in topography resolution, these experiments have deliberately been designed so as to reduce other effects. Consequently, the coarse and fine domain NO_x-emissions have been specified with equal resolution of 1 km². Furthermore, when presenting model results from the simulations, averaged values from the four fine grid cells within one coarse grid cell is compared with the coarse grid cell value.

In figure 3.4a an example of the resulting hourly NO_x-concentrations for a 48 hour simulation period are shown for the lowest 1 km grid cell containing the Carl Berner area, i.e. a central city area in Oslo. Results from three simulations are shown; the coarse grid, the nested fine grid with boundary values from the coarse grid simulation applied at the boundaries, and the same fine grid with no boundary values applied at the boundaries. As seen in this figure large deviations are found between the coarse and the fine grid model results. These deviations are caused by the fact that the applied wind field model generates significant changes in the surface wind pattern in this area as a consequence of the change in topography resolution. Moreover, for this central area the effect of the nesting procedure, i.e. application of coarse grid concentration values at the open boundaries of the nested domain, seems to be of much less importance than the change in the applied wind field.

In figure 3.4b the results from the same experiments as in figure 3.4a are shown for the grid cell covering the south-western part of Bygdøy. This is an area with less topographic variation and with much smaller emission intensities than the Carl Berner area. Because of the low level of local emissions the influence of the nesting procedure is more pronounced for this area. Still, however, the deviations in concentration levels between the coarse grid and the nested fine grid is relatively large, pointing to the fact that even small changes in wind speed and direction can influence concentration estimates severely.

The results from the test experiments shown in figure 3.4a and 3.4b clearly demonstrate the importance of the meteorological input data, especially when performing dispersion modelling in complex terrain areas. A major part of the work in the next phase of this project will therefore be devoted to the further study of how to construct consistent meteorological wind fields for application in nested dispersion models.

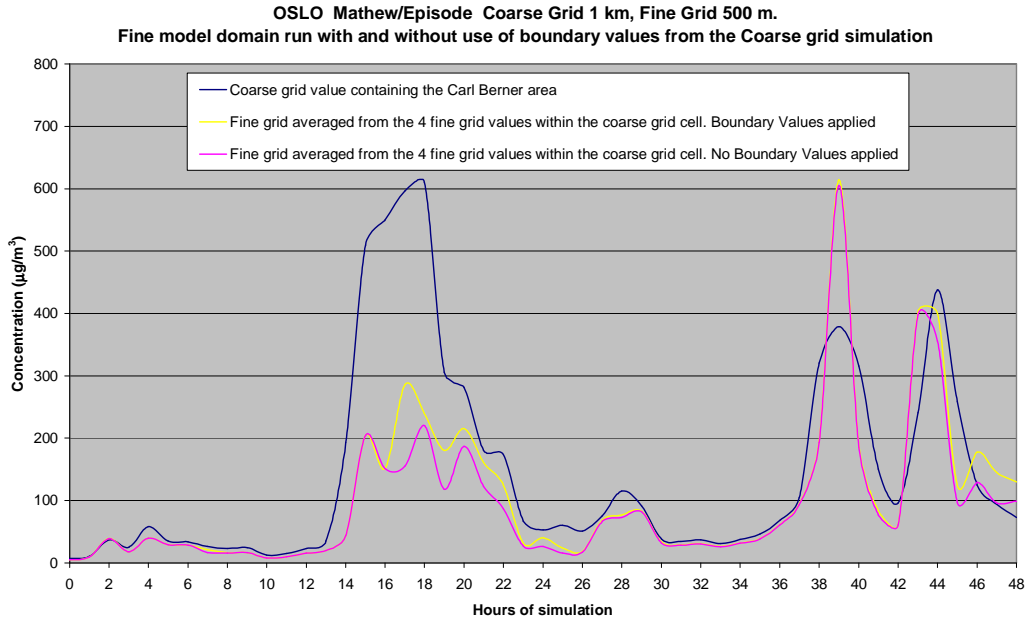


Figure 3.4a: Calculated NO_x concentrations in coarse grid cell containing the Carl Berner area. In addition the averaged values of the four fine grid cell values within this coarse grid cell are presented both when coarse grid values are applied at the open boundaries and when no boundary values are applied.

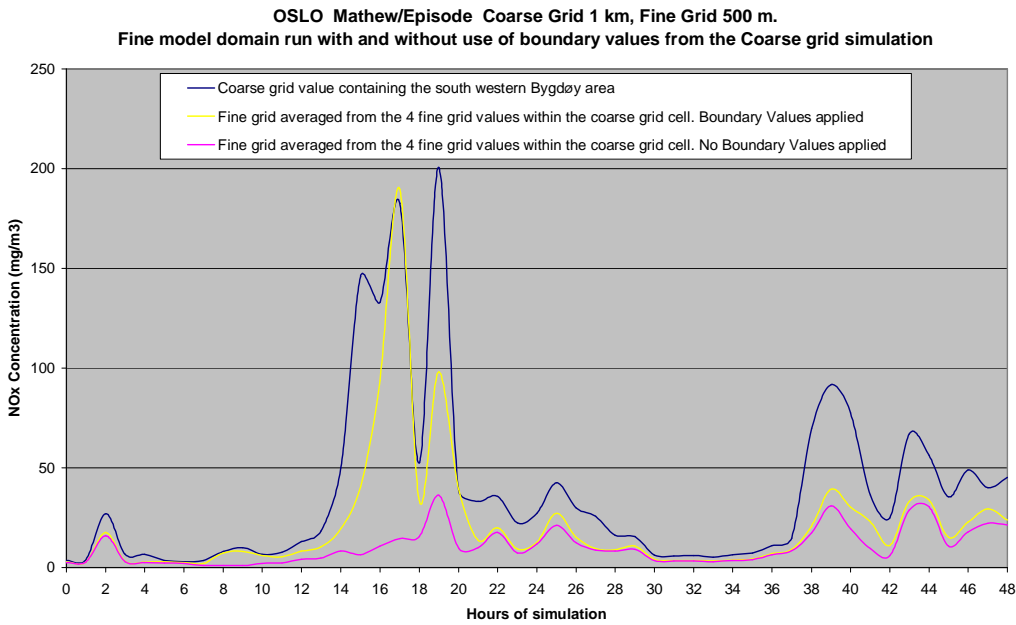


Figure 3.4b: Calculated NO_x concentrations in coarse grid cell containing the south-western part of Bygdøy. As in figure 3.4a the averaged values of the four fine grid cell values within this coarse grid cell are presented both when coarse grid values are applied at the open boundaries and when no boundary values are applied.

4. The nested EMEP/EPISODE model

The next step in the development of a fully nested modelling system has been to couple the self nested EPISODE model with the regional scale EMEP Unified Model and to perform realistic photo-chemical simulations.

To achieve this, the EMEP Unified Model output has been used as boundary conditions for the EPISODE model. These data have a time resolution of 3 hours and a spatial resolution of 50 km. The outer nest of EPISODE uses a temporal resolution of 1 hour and a spatial resolution of 10 km so the EMEP data were bilinearly interpolated spatially and linearly interpolated temporally to match the EPISODE requirements. Only 22 chemical species were specified as boundary conditions for the run, the rest was assumed equal to zero at the outer boundary.

In order to exploit the nesting capabilities of the modelling system, emission inventories with the same resolution as each of the nested grid domains are needed for a large numbers of atmospheric species. If the emissions are given with coarser resolution than the model grid, much of the expected benefits of the increased model resolution are lost. Unfortunately, emission inventories of this quality are not available in the Oslo area at the moment. However, this type of emission inventories has been produced for some European cities. One of these cities is Berlin, and we have therefore in this phase of the project chosen to use this city as a test site for the fully nested modelling system. The required emission data are here available for an area of 300x300 km², covering the city- and suburban-areas of Berlin, as well as large rural areas surrounding the city. Gridded information on area source emissions is available within this area down to a grid scale of about 2 km. In addition the inventory contains detailed information of about 5000 individual point sources.

4.1 The base case experiment

The self nested EPISODE version has been set up for this area with a grid resolution of 10 km for the coarsest grid. Within this domain two finer nests have been defined, one with 5 km resolution and the other with 2.5 km resolution. All of the domains have applied a horizontal grid of 30 x 30 gridcells, and 6 levels in the vertical. For the test experiments presented in the following, the vertical spacing has been equal in all domains. The thickness of the sigma-layers has been (starting from below): 50 m, 100 m, 200 m, 400 m, 800 m, and 1600 m, giving a total model height of 3150 m in the applied sigma-coordinate system.

For each of the point sources the emissions have been introduced at the model height corresponding to the effective plume height. These heights have been calculated using traditional plume rise algorithms (Briggs, 1975). In figure 4.1 the mean distribution of the applied area emissions of NO are presented for the three nests considered. The city of Berlin is clearly seen as a high emission area in the innermost nest. Furthermore, the signature of the emissions from the main road network in and out of the city centre is also visible. The increased emission resolution in each of the three nests is clearly demonstrated in this figure. Note that the locations of the point sources, which are included as white dots in figure 4.1, are distributed all over the three model domains.

Photo-chemical test simulations for the above three nests have then been performed for the month of April 1999, and gridded concentration levels for all of the 45 compounds have been

computed. Hourly concentration values applied at the open boundaries of the coarsest EPISODE grid have been taken from the EMEP Unified Model. Apart from this all of the boundary values for the finer model nests have been computed internally by the EPISODE model. The applied meteorological fields for the three nests have been produced by linear interpolation of the meteorological input to the coarsest nest, and therefore the meteorology does not introduce any significant increase in resolution. Consequently, the differences in the model output are mainly caused by the increased detail in the prescribed emissions applied in each grid.

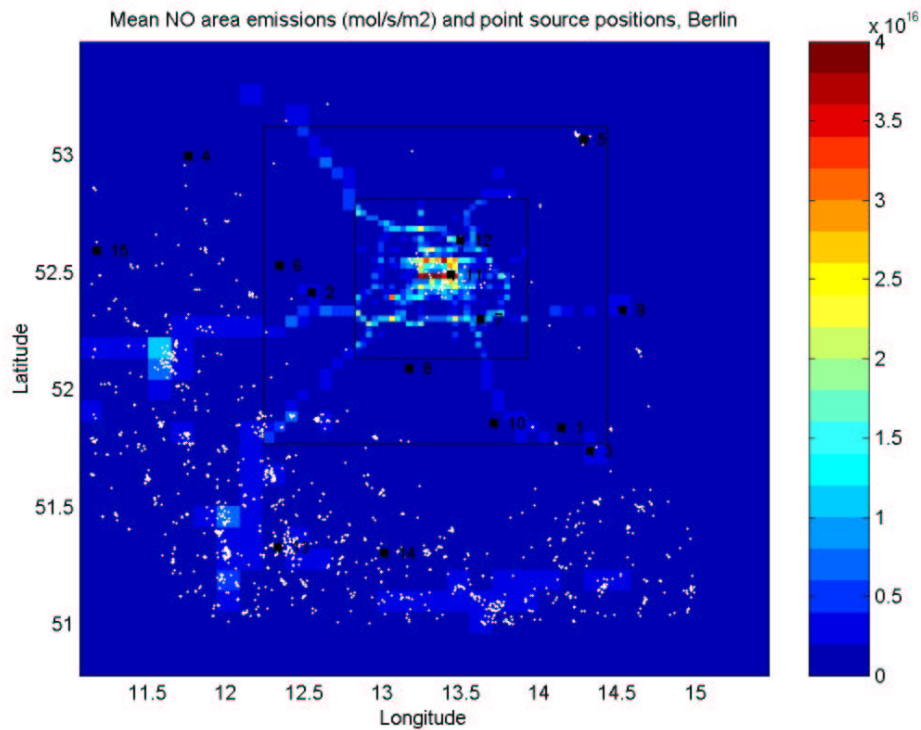


Figure 4.1: The mean area emission distribution of NO in the three model nests applied for the Berlin area. The point source locations are depicted as white dots. The numbered measurement sites are shown as black squares.

In figure 4.2a an example of the calculated hourly ground level O₃ concentration fields for the three nests are presented. The figure shows the situation at 7 p.m. on the 28th of April 1999. The corresponding NO₂ concentration fields are shown in figure 4.2b.

In these figures a plume of NO₂ is seen to stretch out to the south east of the city centre of Berlin, with a corresponding plume of low ozone values. The wind direction is clearly from the north-west in this particular situation. The most pronounced effect of the nesting procedure is the improved spatial details in the computed concentration fields within the finer resolution grids. In the coarser domains, i.e. in the 10 km and 5 km model grids, the various point sources are seen to make significant contributions to the calculated concentration levels.

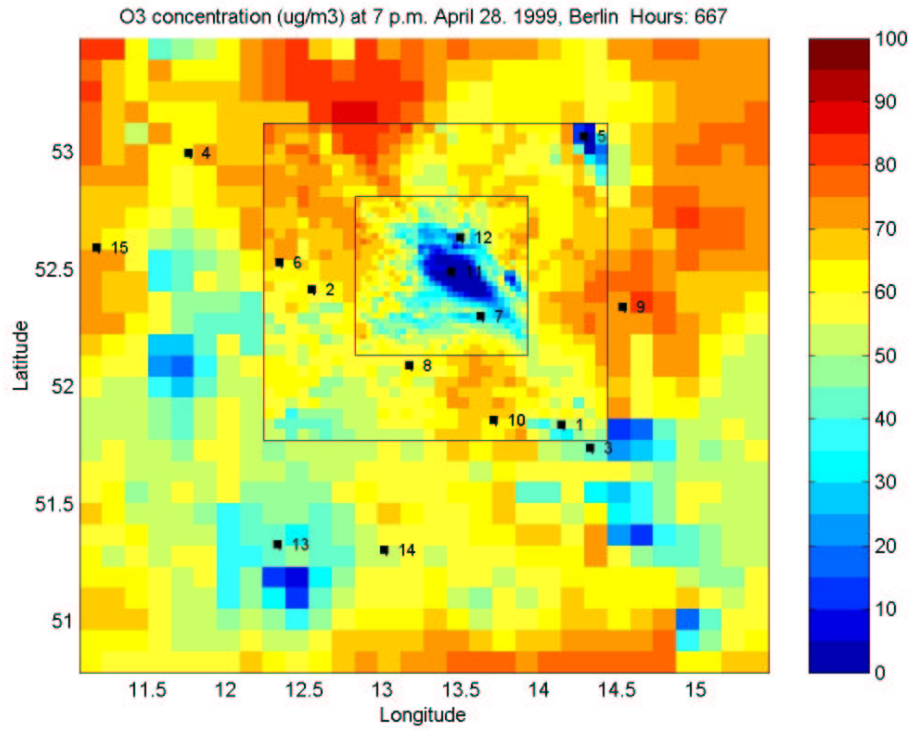


Figure 4.2a: Computed ground level O₃ concentrations at 7 p.m. on April 28th 1999. The positions and numbering of the observation points are depicted in the figure.

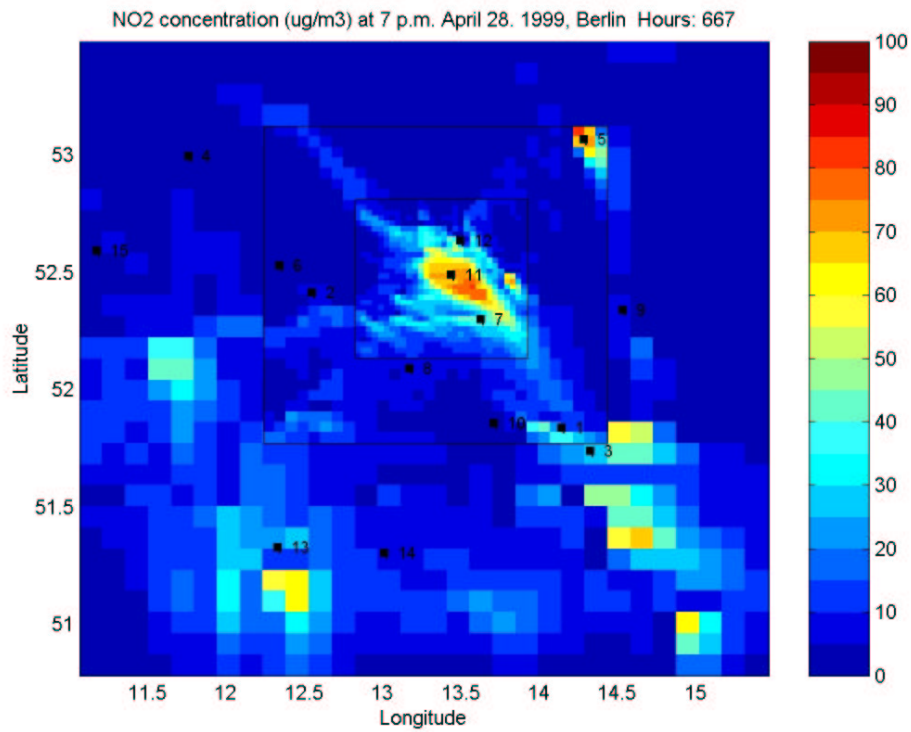


Figure 4.2b: Computed ground level NO₂ concentrations at 7 p.m. on April 28th 1999. The positions and numbering of the observation points are depicted in the figure

In the following we will concentrate our discussion on the comparison of the model calculated concentrations and the measurements available at the three measurement sites 7, 11, and 12 in the figures above. These observations sites are common for all of the three applied nests. With reference to figure 4.1 it is seen that observation site 11 is located in the central Berlin area experiencing the highest NO emissions. Observation point 7 and 12 are situated south-east and north, respectively, of the central point 11 in areas with somewhat less exposure to primary NO emissions. Furthermore, to reduce the complexity of the discussion we will only consider the three compounds of ozone (O_3), nitric oxide (NO), and nitrogen dioxide (NO_2).

In figure 4.3a the time series of hourly computed and observed values of these three compounds are shown for the central observation point 11 for the whole of April 1999. The calculated values at the lowermost grid square containing this observation point are plotted for all of the three nests, and their curves are labelled Grid 1 (10 km^2), Grid 2 (5 km^2) and Grid 3 (2.5 km^2) in figure 4.3a. The general features revealed in this figure is a relatively good agreement between observed and computed O_3 levels, a relatively systematic overestimation of NO, and estimated NO_2 levels that shows varying agreement with the observations throughout the simulation period. The correlation coefficients for the different curves are given in the heading above each of the compound plots in figure 4.3a. These are quite low, i.e. between 0.16 and 0.46, for all of the computed values. However, the agreement between computed and observed values is especially low for the first 6 days of this simulation period. A more detailed examination of the model results have revealed that this most probably is due to a systematic overestimation of the O_3 and NO_2 levels specified at the outer model boundary during this period. The first 5-6 days of April 1999 coincide with a period with persistent wind direction from the east, and it seems like the EMEP model during this period calculate somewhat too high ozone levels over the Berlin model area.

Since these boundary problems add to the complexity of the interpretation of the results, and since they are only found during the first days of this simulation, we have chosen to concentrate the further discussion on the period starting on the 7th of April, continuing to the end of the month. For clarity the corresponding time series for this period is shown in figure 4.3b, with the new correlation coefficients for this shorter period given in the headings. By not considering the first six days of the month it is seen that the correlation coefficients improve significantly for all three compounds. The correlation of O_3 now varies between 0.51 and 0.59, while the correlations for NO and NO_2 are found in the range 0.33 to 0.48, for this observation site. An interesting feature revealed by these results is that the increase in model resolution does not seem to improve the value of the correlation coefficients. For both O_3 and NO the correlation actually decreases when the grid values of the finer nests are considered, while the correlation for NO_2 for the finer nests are almost identical. These findings may seem disappointing since the idea of creating a nested modelling system basically was motivated by the desire of being able to estimate realistic concentration distributions in urban areas or areas in the vicinity of primary pollutant sources. However, before one draws too strong conclusions based on these correlation estimates, one should note that the observation data are only measured at a single urban point, and that it is compared with grid box averaged values of varying, but still considerable, size. In order to make a more confirmative comparison between model results and observed values in such urbanized areas, more detailed information on the spatial variability of the observed concentration levels, i.e. within the scale of the grid spacing, is necessary. At the moment we do not have this information.

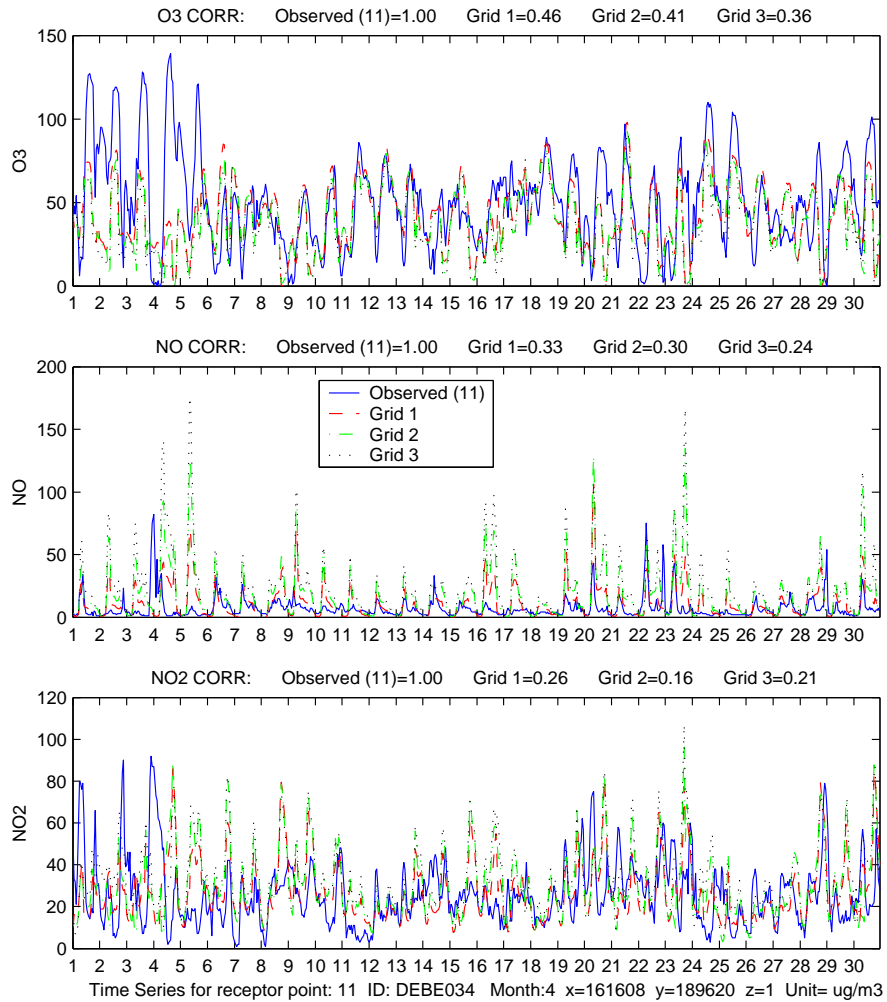


Figure 4.3a: Hourly time series of the observed and calculated concentrations of O_3 , NO and NO_2 for the month of April 1999, for the central city observation point 11. The receptor point value has been calculated for each of the three model domains. Grid 1, 2, and 3 is the nests with 10, 5, and 2.5 km resolution, respectively. The calculated correlation coefficients for the different nests are given in the heading above each figure.

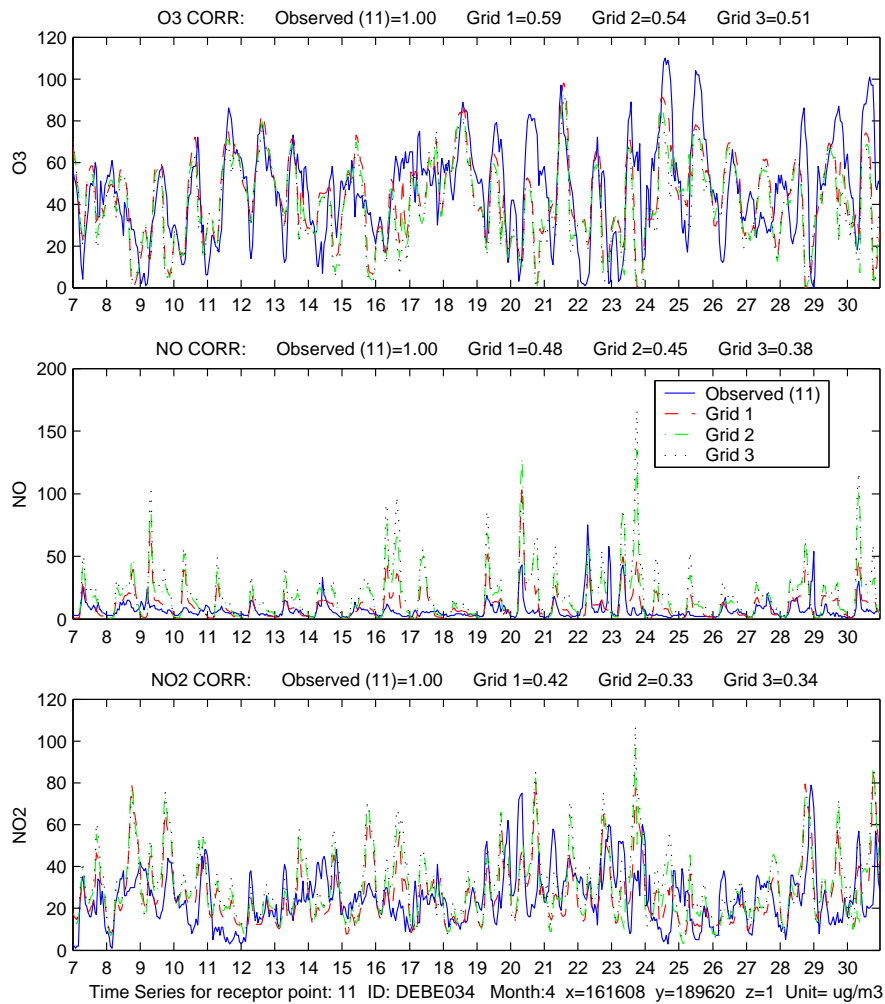


Figure 4.3b: Hourly time series of the observed and calculated concentrations of O_3 , NO and NO_2 for the period from the 7th to the 30th. of April 1999, for the central city observation point 11. The receptor point value has been calculated for each of the three model domains. Grid 1, 2, and 3 is the nests with 10, 5, and 2.5 km resolution, respectively. The correlation coefficients for the different grids are given in the heading above each figure.

Additional information on the differences between the results from the various model nests can be visualized by constructing curves showing the average daily cycle for the grid square values that are compared with the observational data. For observation point 11 such curves are shown in figure 4.3c below. The average daily cycles shown in figure 4.3c are based entirely on the hourly computed and observed values for the period 7th – 30th April 1999, i.e. the data shown in figure 4.3b. In the heading of each of the plots in figure 4.3c the mean values for this period are also presented.

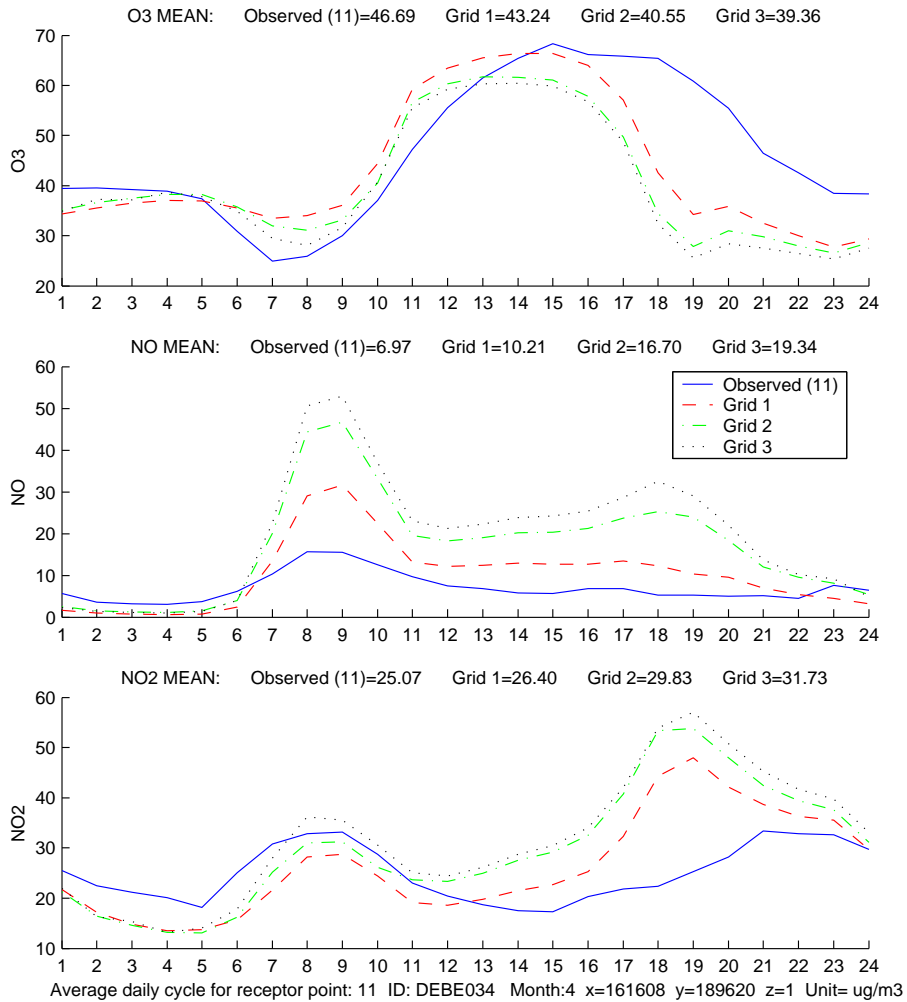


Figure 4.3c: The average daily cycle of the observed and calculated concentrations of O₃, NO and NO₂ for the central city observation point 11. The curves are calculated as averages over the period from the 7th of April 1999 to the end of the month and thus correspond to the time series data in figure 4.3b above. The mean observed and calculated values for this period are given in the heading above each figure.

By combining the information shown in figure 4.3b and 4.3c it is seen that the computed NO levels are systematically higher during daytime than the measured values at this observation point. Furthermore, the increased model resolution leads to significantly higher NO concentrations. Note also that the differences in computed NO levels between the coarse grid and the finer nests are equally large, or even larger, than the difference between the coarsest grid and the observations. This may indicate that the observation point is deliberately located in an area of minimum local sources, a hypothesis that is supported by the surprisingly low NO levels measured at this observation point. Of the three compounds shown, it is expected that NO will be most strongly influenced by changes in emission resolution. This is also confirmed in the model results shown figure 4.3c.

A systematic feature seen at all observation points, is that the model calculated maximum daily O₃ levels, and the afternoon peak in NO₂ levels, seem to fall off too early in the afternoon. One reason for this misfit may be linked to a systematic error in the timing of the build-up of the afternoon stable boundary layer. Other possibilities are that it is either caused by inaccuracies in the chemistry scheme or the applied time variations of the emissions. More detailed studies are necessary in order to clarify this point.

The results presented in figures 4.3b and 4.3c are reproduced for observation point 7 in figures 4.4a and 4.4b, and for observation point 12 in figures 4.5a and 4.5b. Since the observational data of O₃ were not available for observation point 12 the correlation coefficient for O₃, given in figure 4.5a as zero, is not valid.

The most marked difference between the model results at observation point 7 (see figures 4.4a and 4.4b), as compared to the results at point 11, is the small variations in the concentration levels from the different nests. This shows that the applied emission inventory does not vary much in the different grid resolutions in this area. The correlation of O₃ is at its best at this location with values varying between 0.66 and 0.69, while the correlations for NO and NO₂ are approximately unaltered, ranging from 0.32 to 0.40. Again no improvement is seen in the correlations as a result of the increase in resolution. A special feature at observation point 7, and in contrast to both the results at observation point 11 and 12, is that the morning peak in the average daily cycle of NO is clearly underestimated in the model results. As seen in figure 4.4a this feature is caused by 4 to 5 morning peak values that are not captured in the model results. Moreover, the results at observation point 7 also depart from the results at observation point 11 and 12 in that the model results tend systematically to underestimate the observed NO₂ levels. The general feature of too early decline in the modelled O₃ levels, and two early maximum NO₂ levels in the afternoon are evident at all observation points.

The model results at observation point 12 show much resemblance with the results at point 11. A notable difference, however, is that the largest NO concentrations now are computed in the coarsest grid, while the lowest values were found in this grid at observation point 11. This finding confirms that the model results clearly react to local variations in primary emissions of NO. Note from figure 4.5a that the highest correlation for NO and NO₂ are found for this station, ranging between 0.51 and 0.6, again with no general improvement seen as a result of increased resolution.

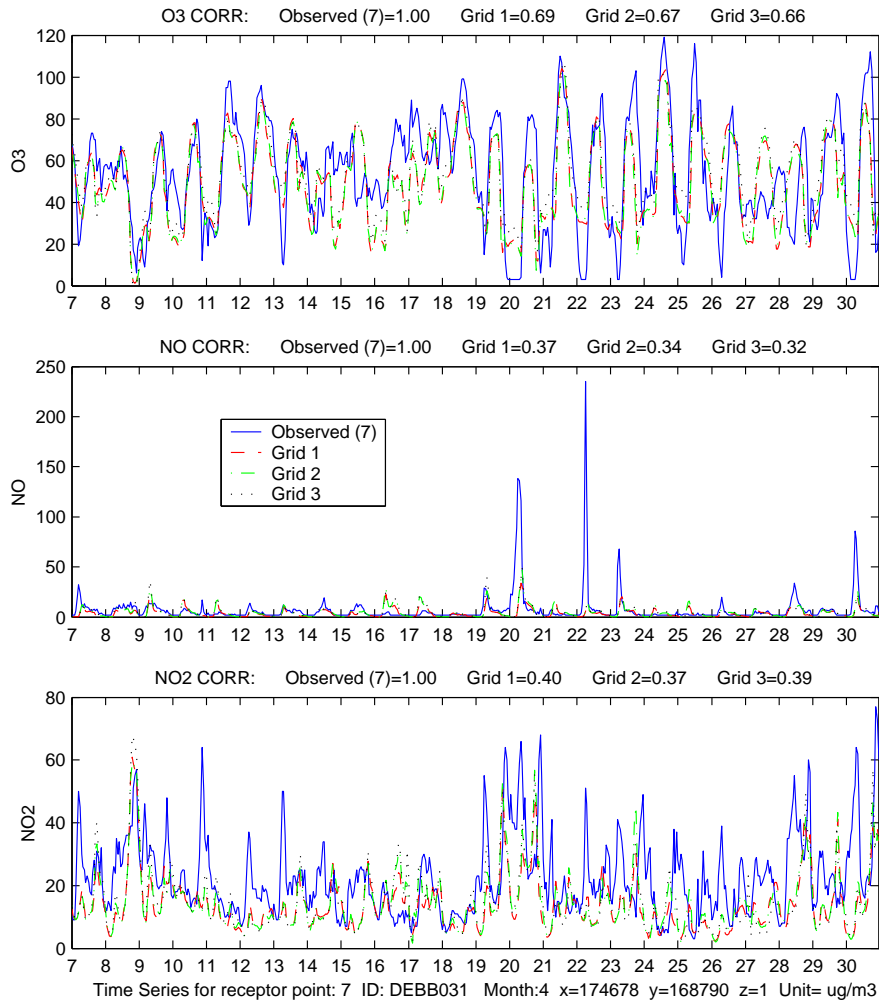


Figure 4.4a: Hourly time series of the observed and calculated concentrations of O_3 , NO and NO_2 for the period from the 7th to the 30th of April 1999, for observation point 7 (south-east of the city centre). The receptor point value has been calculated for each of the three model domains. Grid 1, 2, and 3 is the nests with 10, 5, and 2.5 km resolution, respectively. The correlation coefficients for the different grids are given in the heading above each figure.

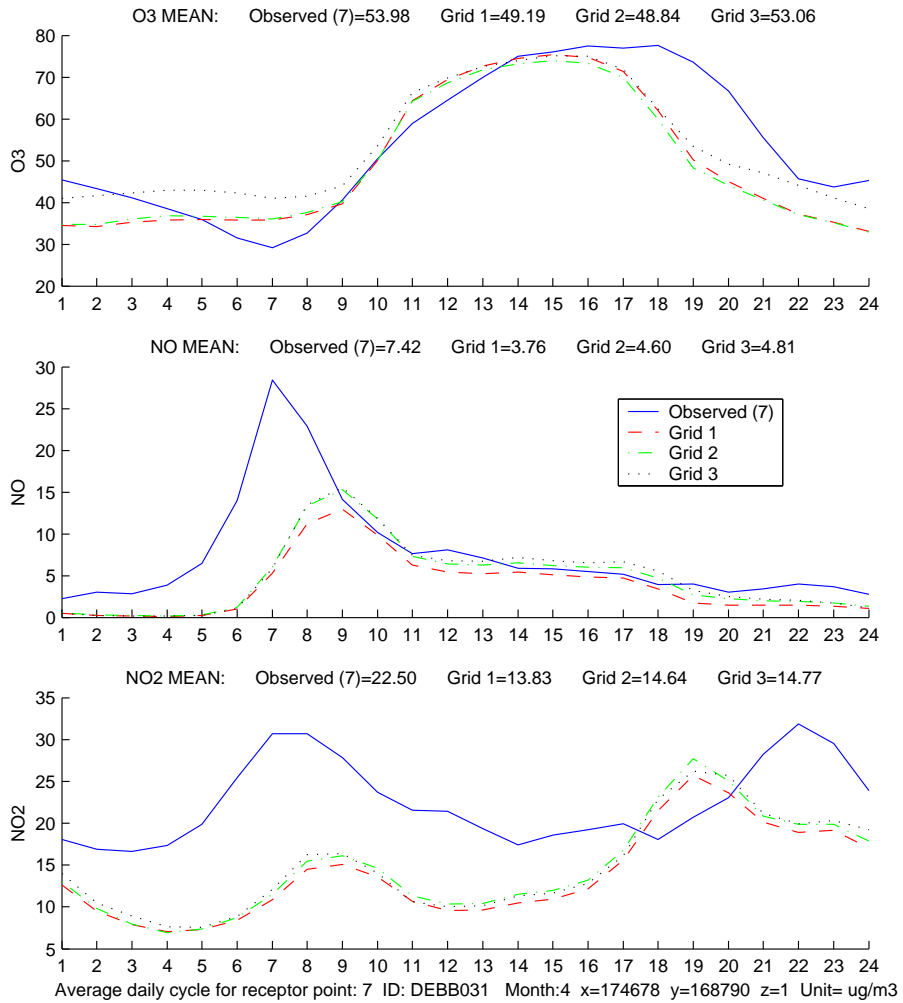


Figure 4.4b: The average daily cycle of the observed and calculated concentrations of O_3 , NO and NO_2 for the central city observation point 7. The curves correspond to the time series presented in figure 4.4a above. The mean observed and calculated value is given in the heading above each figure.

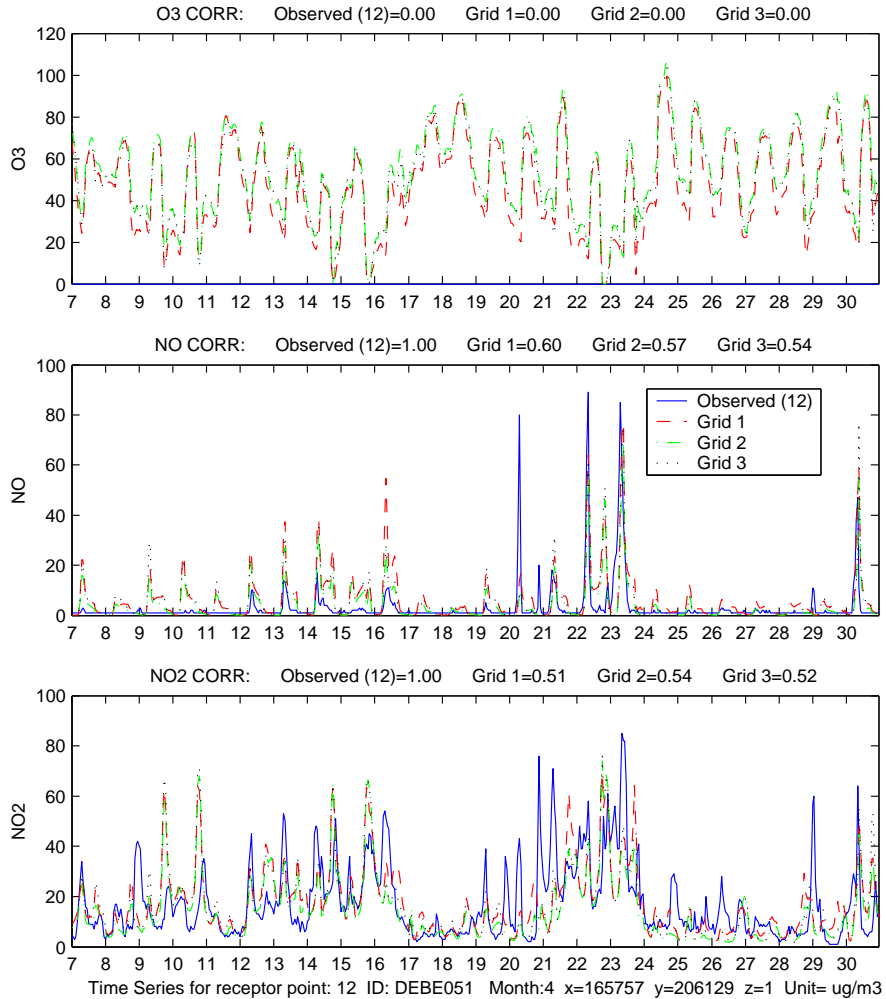


Figure 4.5a: Hourly time series of the observed and calculated concentrations of O_3 , NO and NO_2 for the period from the 7th to the 30th of April 1999, for observation point 12 (just north of the city centre). The receptor point value has been calculated for each of the three model domains. Grid 1, 2, and 3 is the nests with 10, 5, and 2.5 km resolution, respectively. The correlation coefficients for the different grids are given in the heading above each figure. Note that the observations of O_3 are missing at this site.

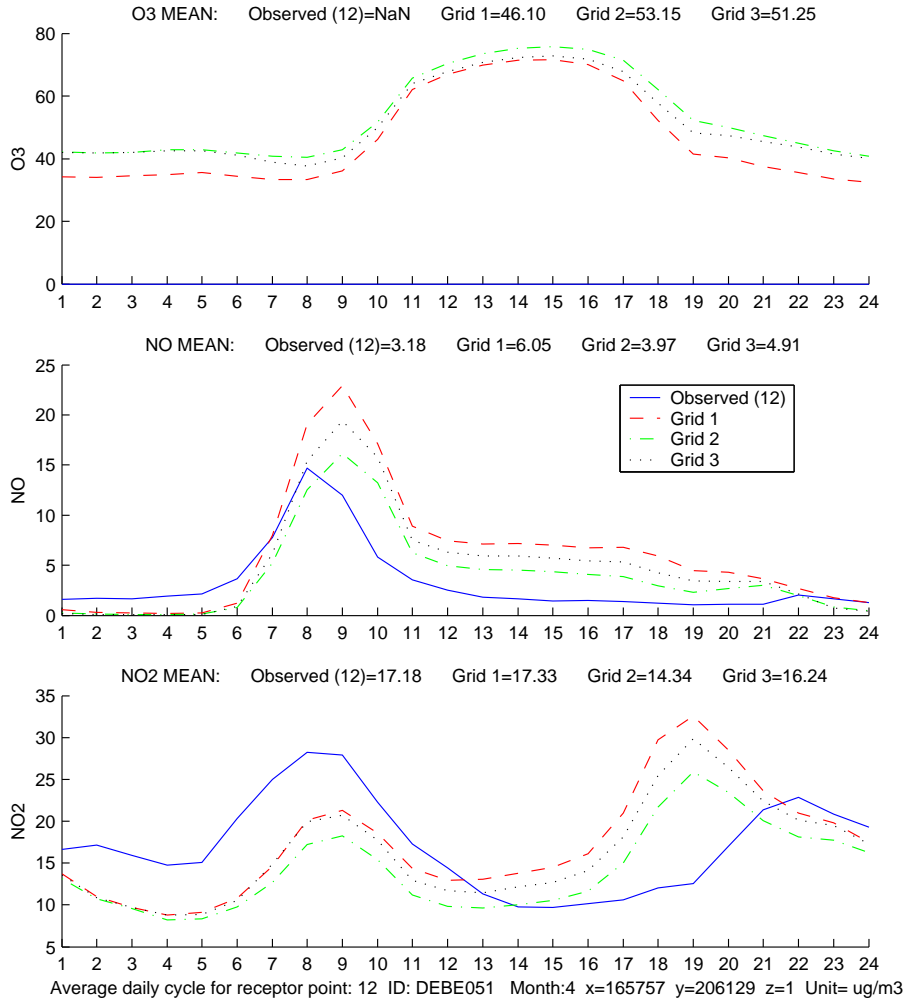


Figure 4.5b: The average daily cycle of the observed and calculated concentrations of O_3 , NO and NO_2 for the central city observation point 12. The curves correspond to the time series presented in figure 4.5a above. The mean observed and calculated value is given in the heading above each figure.

4.2 Sensitivity experiments

In order to investigate the effects of both the nesting procedure and the emission resolution, the following two sensitivity tests have been performed.

1. The nesting procedure has been tested by simply skipping the two coarsest model domains, and applying the interpolated EMEP boundary values directly at the open boundaries of the innermost model domain, i.e. the domain with grid resolution of 2.5 km.
2. The effect of the increased resolution in the emission fields has been tested by applying the emission inventory with 10 km resolution for all of the three model domains. Except for this aggregation of the emissions, the nesting procedure has been applied as above to calculate the concentration values in the different grids.

The results from the above two sensitivity tests are shown for observation point 11 in figures 4.6a and 4.6b below. Time series (figure 4.6a) and the average daily cycle (figure 4.6b) of the observations, the original 10 km (labelled: Grid 1) results, the original 2.5 km (labelled: Grid 3) results, the new Grid 3 results with 10 km emission inventory (labelled: Grid 3 AGG Emissions), and the new Grid 3 results with EMEP boundary values (labelled: Grid 3 EmepBC) are shown in these plots. The curves showing the observations and the Grid 1 results are included just to facilitate comparisons with the related site 11 plots shown in figures 4.3a and 4.3b. In order to show more clearly the differences of the Grid 3 model results, the time series of these three curves (shown in figure 4.6a) are reproduced in figure 4.6c.

The conclusions to be drawn from the two sensitivity tests are most clearly demonstrated by reference to the curves in figure 4.6b. The results obtained by applying the 50 km resolution EMEP boundary values directly as boundary conditions for the innermost 2.5 km grid are almost identical with the original Grid 3 results from the finest domain in the fully nested three-grid simulation. The largest deviations are found for the maximum daytime O₃ levels since these values are of more secondary origin and in urban areas to a large extent are governed by the inflow from the surrounding areas. For the more locally influenced components of NO and NO₂ the results from these simulations are hardly distinguishable, showing clearly the minor importance of including the nesting procedure in this particular case. Note, however, that this does not mean that the quality of the boundary values is unimportant. It only means that in this situation the nesting procedure does not lead to a significant change in the boundary values finally applied at the open boundaries of the 2.5 km resolution grid.

Comparing the Grid 3 results obtained with the aggregated 10 km emissions in figure 4.6b (dotted curve denoted Grid 3 Agg Emissions) with the other two Grid 3 curves show clearly the important effect of the increased emission resolution at this central urban site.

The sensitivity results have also been investigated for observation points 7 and 12. However, the same general features were found at these sites as at station 13, and these results are therefore not presented as separate figures in this report.

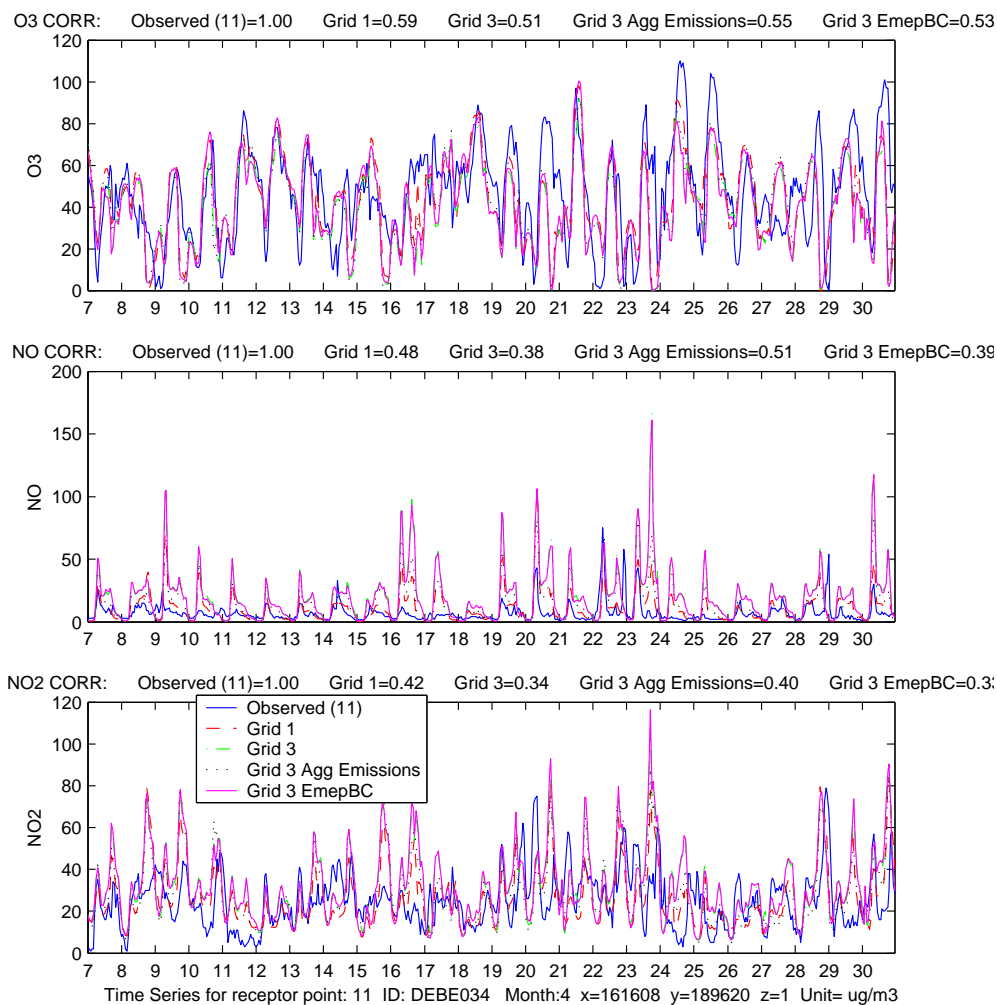


Figure 4.6a: Hourly time series of the observed and calculated concentrations of O_3 , NO and NO_2 for the period from the 7th to the 30th of April 1999, for the central city observation point 11. The receptor point value has been calculated for the coarsest and the finest grids, i.e. the nests with 10 and 2.5 km resolution, respectively. Grid 3 results are also shown when EMEP-values are used directly on the Grid 3 boundaries (EmepBC), and when emissions with 10 km resolution are used in all 3 nests (Agg. Emissions). The correlation coefficients for the different grids are given in the heading above each figure.

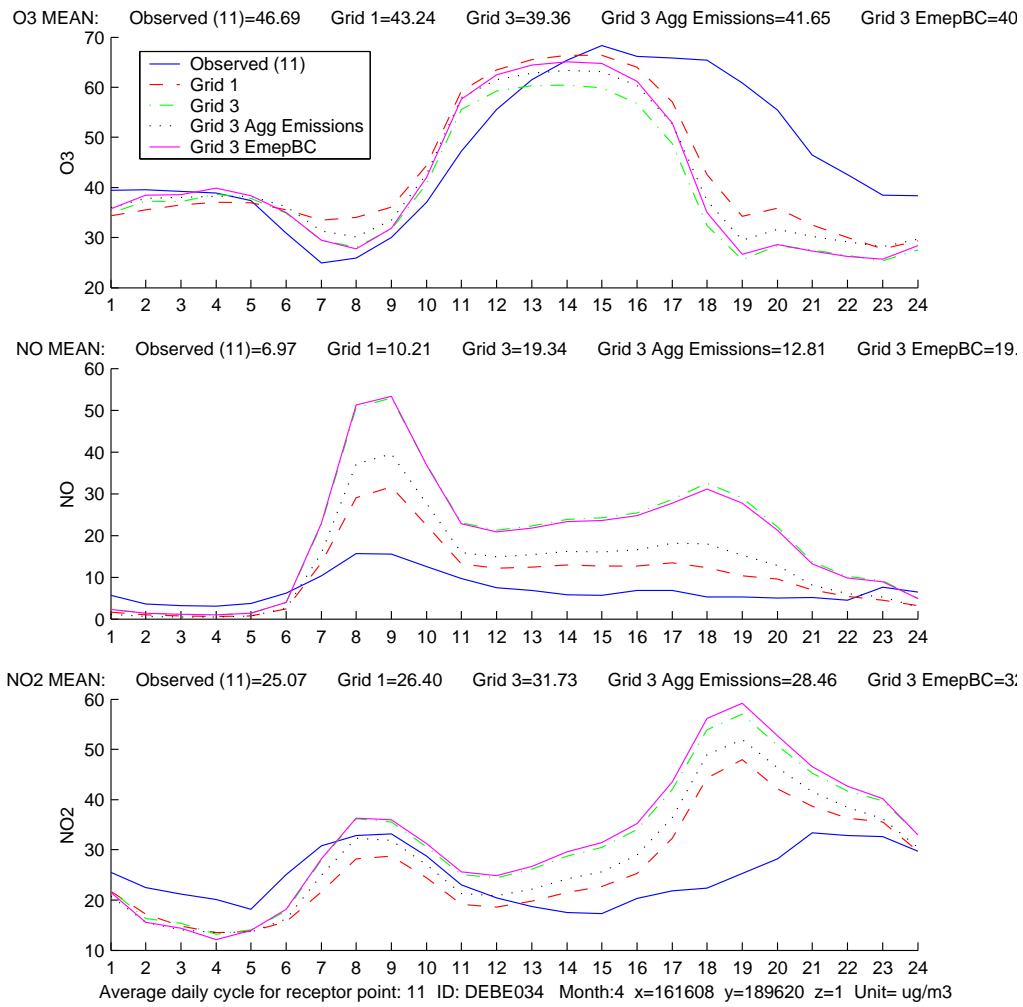


Figure 4.6b: The average daily cycle of the observed and calculated concentrations of O_3 , NO and NO_2 for the central city observation point 11. The curves correspond to the time series presented in figure 4.6a above. The mean observed and calculated value is given in the heading above each figure.

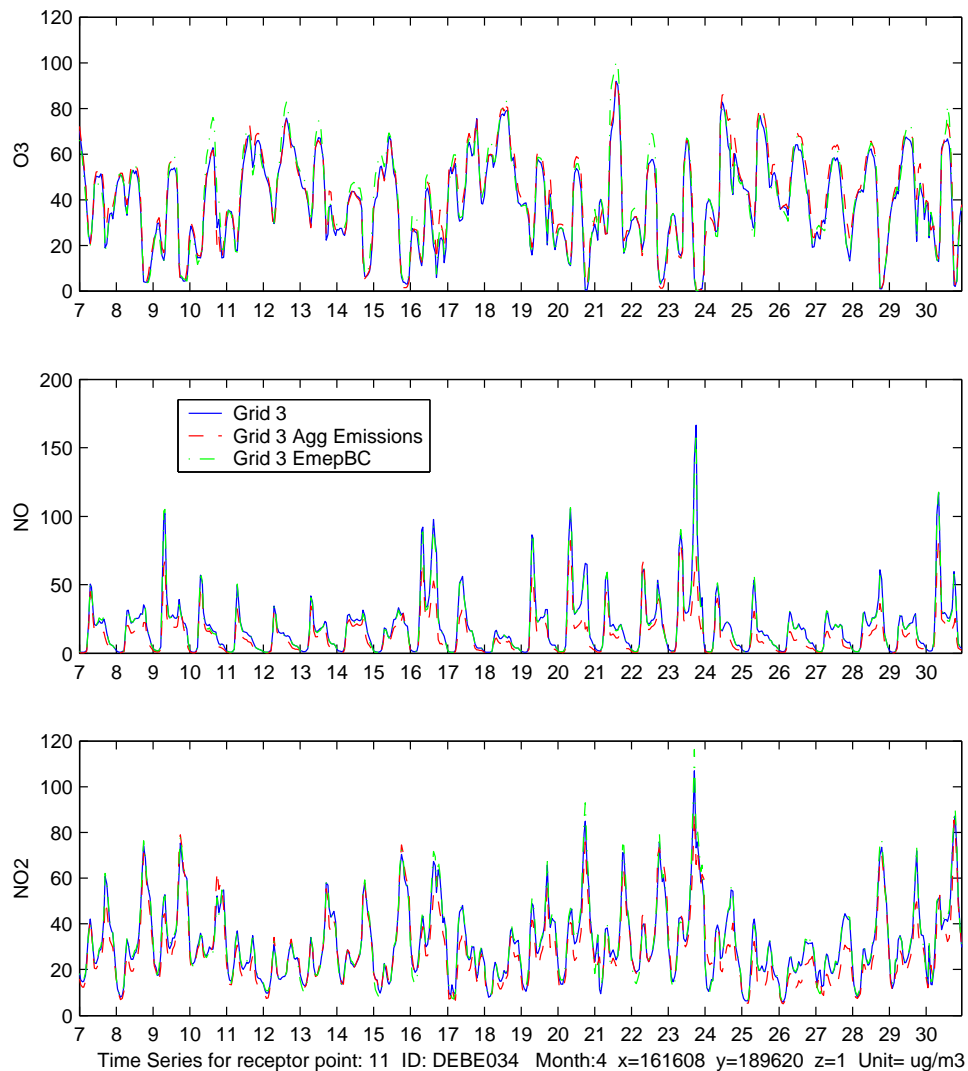


Figure 4.6c: Hourly time series of the observed and calculated concentrations of O_3 , NO and NO_2 for the period from the 7th to the 30th of April 1999, for the central city observation point 11, i.e. similar as figure 4.6a, except that only the Grid 3 results are shown.

4.3 Conclusions and recommendations based on the Berlin test experiments

It should be emphasized that the above findings are valid for the spring conditions during which the above simulations have been performed. Further test experiments, including treatment of summer conditions with stronger photo-chemical activity, as well as winter situations with lower solar intensity and distinctly different boundary layer stability conditions, are needed in order to gain the necessary quality confidence in the new modelling

tool. However, the results obtained so far with this system are promising in that no unphysical results have been found. Moreover, comparison with measurements show that the nested modelling system reproduce observed levels within reasonable bounds, depending, as expected, on component and location. Increased misfits between individual point observations and model calculated grid averages are to be expected for compounds that exhibit large variation over small spatial scales in heavily polluted areas. This is partly due to uncertainties in the model results, but also to a large extent caused by uncertainties in the spatial representativity of the observed values. Moreover, the relatively low levels of NO and NO₂ observed at the urban measuring sites, 11, 7 and 12, indicate that these stations are located in shielded areas with relatively long distance to major urban pollution sources. Although the results from the nested domain did not show any detectable improvement in the statistical measures of the point by point comparisons with observed values, the nest results clearly demonstrated the ability to produce more realistic detail in the computed concentration distributions in response to increased resolution in the emission inventories.

5. Conclusions and remaining tasks

This report presents a detailed description of the various model developments that have been implemented in the urban dispersion model EPISODE and the regional scale Unified EMEP model, in order to facilitate one-way nesting functionality.

A new coordinate system has been implemented in EPISODE as described in section 3.1. Furthermore, a simplified version of the EMEP chemistry has been implemented in this model motivated by the fact that EPISODE will be run for more polluted regions, whereas the EMEP model also needs to cover clean background chemistry. Two main simplifications were used in this work: firstly, RO_2+RO_2 reactions were omitted and secondly, the isoprene mechanism was simplified. With these two types of simplifications a condensed EMEP mechanism with the number of components reduced from 70 to 45 and the number of reactions reduced from about 150 to about 70 was obtained. Test calculations with a box model showed only minor differences between the full and simplified mechanism under moderately anthropogenic polluted conditions.

A two-step Gauss-Seidel integration technique has been applied in the implementation of this chemical scheme into EPISODE model.

The nesting systems developed at NILU and MET.NO are now operational and the work has reached a testing phase. Several simulations have been performed thereby demonstrating that the EPISODE and the EMEP models can be used in a nesting procedure and that EPISODE can apply background concentrations provided by the EMEP model. Both models are behaving as expected and no unphysical effects have been observed so far.

The two models use a nesting procedure based on updates of boundary concentrations. In idealized simulation this procedure has proven to be stable. The EPISODE model has used comparisons with an analytical solution and no spurious effects have been found at the boundaries due to the nesting (section 3.3.2). The nested EMEP model has been applied around Oslo with two different grid resolutions (section 2.3.1). Comparison of the results showed only minor differences between a nested and a direct calculation. This is also a clear indication that the nesting in itself does not introduce new features to the results.

The simulations presented in section 2.3.2 (and 3.3.3) showed that even for a relatively large grid ($1000 \times 1000 \text{ km}^2$), the pollutants with an origin outside of the grid have a strong influence on the pollution levels within the grid area. In the nesting system, all the processes occurring outside the grid are modelled by imposing the concentration levels at the boundaries. These boundary concentrations are updated according to the results obtained in a larger and coarser grid. The rate of update of the boundary concentrations which is required in a nested run will depend on several factors: It is dependent on the resolution, because the resolution of the inner grid will have an influence on the time it takes for the pollutants in a gridcell to be shifted. The size and the geographical position will also have an influence on the timescale on which the different processes occur. For large domains like the EMEP area, the boundary concentrations do not need to be updated often (currently once every month), because the incoming fluxes are determined by processes occurring in other continents and the concentrations are largely stabilized when coming to the EMEP area. For scales of the order

of thousand kilometres, the typical scales are of hours, whereas for local scales the timescales can be much smaller, depending on the distance to the emission sources. The season and meteorological conditions will also have some importance.

The minimum rate of update in a nesting system must be therefore determined for each application, and will depend on the particular situation and quantities of interest. Of course if there is a doubt, a small update frequency can always be chosen; this will never deteriorate the solution, but will increase the computational cost in terms of storage requirements.

The EMEP and EPISODE nesting systems are so-called off-line, i.e. the concentrations are computed separately in the coarse and fine grids; the relevant concentrations in the coarse grid are stored in order to be used by the fine grid. Also the meteorological data are computed and stored independently from the air pollution model runs. Compared with an on-line system, the disadvantage of an off-line system is the requirement of large storage capacity and this may in turn limit the rate of updates of the boundary concentrations. In our simulations the rate of updates was large enough and the storage capacity has not proven to be a limitation. The nesting of EPISODE with boundary conditions provided by the EMEP model must be done off-line, since the two models are used independently.

A fundamental choice which must be done before starting a nested simulation is the determination of grid sizes and grid resolutions. Often this choice is determined by the availability of meteorological and emission data. In systems where the meteorological data is computed dynamically (or on-line), the choice of the size of the nested grids have to take into account the requirements of the meteorological model. It is common to choose successive grid resolutions decreasing with a factor three for each nested grid. In air pollution models a factor three may be too restrictive, and the nesting can be achieved more effectively by choosing a larger stride between the nested grids. For specific applications it is preferable to construct meteorological and emissions data specially dedicated to the needs of the nested air pollution model. This presupposes that the consequences of choosing different grids are known.

In the simulations presented in section 2.3.1, there were no significant differences in the results when changing only the grid resolution without changing the meteorological and emission information. The effect of using more refined emission data was investigated using EMEP model (section 2.3.3) and EPISODE (section 4.1). Very close to strong emission sources the effect of improved emission description was clearly visible. This demonstrates the necessity of using high resolution grids for the description of urban areas. On the other hand, at positions which are not in the immediate vicinity of large sources, the results showed surprising small differences when refining the description of the emissions. For a regional model, aiming at providing background concentrations for use as boundary concentration in a local model, the accurate description of air pollution close to large sources is not the main priority. Therefore the provisional conclusion is that the embedding grid can have a much coarser resolution than first assumed. Only the innermost grid containing the main sources of interest (urban centre for instance), needs to be described with highest resolution. This is also observed directly in the test presented in section 4.2. There it was shown that the EPISODE model applied on a grid with a resolution of 2.5 km gave very similar results when using a successive nesting with 50-10-5-2.5 km or applying directly the 50 km grid onto the 2.5 km grid. It is however important to note that these are only preliminary results valid only for the specific cases tested here. More testing is needed before general conclusions can be drawn. In particular in the future the tests must be performed on longer timescales covering winter and summer months.

Another fundamental parameter which needs to be tested is the effect of the choice of meteorological data. In most of the simulations presented in this work the meteorological data was interpolated down to the different grid resolutions. A more correct approach would be to calculate directly the meteorological data in each grid. The tests presented in section 3.3.3, using Mathew/EPISODE show that large differences can be expected by changing the description of the meteorology. At met.no different meteorological drivers are being evaluated. The testing of HIRLAM50, HIRLAM20, MM5 and ECMWF meteorological data will be a central part in the next phase of this project.

References

Benedictow A., 2003, *Documentation and verification of the 1980 PARLAM-PS meteorological fields used as input to the Eulerian EMEP model.*

Documentation and verification of the 1985 PARLAM-PS meteorological fields used as input to the Eulerian EMEP model.

Documentation and verification of the 1995 PARLAM-PS meteorological fields used as input to the Eulerian EMEP model.

Documentation and verification of the 1999 PARLAM-PS meteorological fields used as input to the Eulerian EMEP model.

Documentation and verification of the 2000 PARLAM-PS meteorological fields used as input to the Eulerian EMEP model.

Documentation and verification of the 2001 PARLAM-PS meteorological fields used as input to the Eulerian EMEP model.

Research Report (to be published), Norwegian Meteorological Institute, Oslo, Norway.

Berge E., and Jakobsen H. A., (1998) A regional scale multi-layer model for the calculation of long-term transport and deposition of air pollution in Europe. *Tellus*, **50B**, 205-223.

Briggs, G.A. (1975) Plume Rise Predictions. In: *Lectures on Air Pollution and Environmental Impact Analysis*. Ed. by D.A. Haugen. Boston, MA., Amer. Meteorol. Soc. pp. 59-111.

CityDelta web pages: <http://rea.ei.jrc.it/netshare/thunis/citydelta>

EMEP, 2003, *Part I, EMEP Unified Eulerian modell. Model description*. Norwegian Meteorological Institute, Oslo, Norway, EMEP/MSC-W Report 1/2003.

EMEP, 2002, *Transboundary Acidification, Eutrophication and Ground Level Ozone in Europe*, Norwegian Meteorological Institute, Oslo, Norway, EMEP/MSC-W Report 1 and 2/2002.

Foster, F., Walker, H., Duckworth, G., Taylor, A. and Sugiyama, G. (1995). User's guide to the CG-MATHEW/Adpic models, Version 3.0. Lawrence Livermore National Laboratory (Report UCRL-MA-103581 Rev. 3).

Grønskei, K.E., Walker, S.E. and Gram, F. (1993) Evaluation of a model for hourly spatial concentrations distributions, *Atmos. Environ.*, **27B**, 105-120.

- Holstad, A. and Lie, I. , 2002 , On the computation of mass conservative wind and vertical velocity fields, Research Report No. 141, Norwegian Meteorological Institute, Oslo, Norway.
- IUPAC, (2001) International Union of Pure and Applied Chemistry
- Olendrzynski K., Berge E., and Bartnicki J., (2000) EMEP Eulerian acid deposition model and its applications. *Journal of Operational Research*, **122**, 426-439.
- Sherman, C.A. (1978). A mass consistent model for wind fields over complex terrain. *J. Appl. Meteorol.*, *17*, 312-319.
- Simpson, D. (1995). Biogenic emissions in Europe, 2, Implications for ozone control strategies, *J. Geophys. Res.*, **100**, 22891-22906.
- Slørdal, L. H. (2002). Applying model calculations to estimate future urban air quality with respect to the requirements of the EU directives on NO₂ and PM₁₀. In: *Proceedings of the Second Conference on Air Pollution Modelling and Simulation*. Ed. by B. Sportisse. Berlin, Springer. p. 89-100.
- Slørdal, L. H. (2002). MATHEW as applied in AirQUIS/EPISODE. Model description. Kjeller, Norwegian Institute for Air Research (NILU TR 09/2002).
- Slørdal L.H., Solberg S., and Walker S.E. (2003) The Urban Dispersion Model EPISODE. Technical description. (NILU TR../03) In press.
- Verwer J. G. and Simpson D., (1995) Explicit methods for stiff ODEs from atmospheric chemistry. *Applied Numerical Mathematics*, *18*, 413-430, 1995.
- Walker SE, Slørdal LH, Guerreiro C, Gram F and Grønskei KE (1999) Air Pollution exposure monitoring and estimation. Part II. Model evaluation and population exposure. *J. Environ. Monit*, *1*, pp 321-326.
- Wind, P., Tarrason, L., Berge, E., Slørdal, L.H., Solberg, S. and Walker, S.E. (2002) Development of a modelling system able to link hemispheric-regional and local air pollution. *Joint MSC-W & NILU Note 5/02*. Oslo, The Norwegian Meteorological Institute. http://www.emep.int/reports/emep_note_5_2002.pdf